Forces between solid surfaces in aqueous electrolyte solutions

Smith, Alexander; Borkovec, Michal; Trefalt, Gregor

How to cite

SMITH, Alexander, BORKOVEC, Michal, TREFALT, Gregor. Forces between solid surfaces in aqueous electrolyte solutions. In: Advances in Colloid and Interface Science, 2020, vol. 275, p. 102078. doi: 10.1016/j.cis.2019.102078

This publication URL: https://archive-ouverte.unige.ch//unige:136316
Publication DOI: 10.1016/j.cis.2019.102078

Revised, October 11, 2019

Published in Adv. Colloid Interface Sci. 275, 102078 (2020)

DOI: 10.1016/j.cis.2019.102078

Forces between solid surfaces in aqueous electrolyte solutions

Alexander M. Smith, Michal Borkovec, Gregor Trefalt*

Department of Inorganic and Analytical Chemistry, University of Geneva, Sciences II,

30 Quai Ernest-Ansermet, 1205 Geneva, Switzerland

*Corresponding author, Email. gregor.trefalt@unige.ch

Abstract

This review addresses experimental findings obtained with direct force measurements between two similar or dissimilar solid surfaces in aqueous electrolyte solutions. Interpretation of these measurements is mainly put forward in terms of the classical theory of Derjaguin, Landau, Verwey, and Overbeek (DLVO). This theory invokes a superposition of attractive van der Waals forces and repulsive double layer forces. DLVO theory is shown to be extremely reliable, even in the case of multivalent ions. However, such a description is only successful, when appropriate surface charge densities, charge regulation characteristics, and ion pairing or complexation equilibria in solution are considered. Deviations from DLVO theory only manifest themselves at distances of typically below few nm. More long-ranged non-DLVO forces can be observed in some situations, particularly, in concentrated electrolyte solutions, in the presence of strongly adsorbed layers, or for hydrophobic surfaces. The latter forces probably originate from patch-charge surface heterogeneities, which can be induced by ion-ion correlation effects, charge fluctuations, or other types of surface heterogeneities.

Graphical Abstract

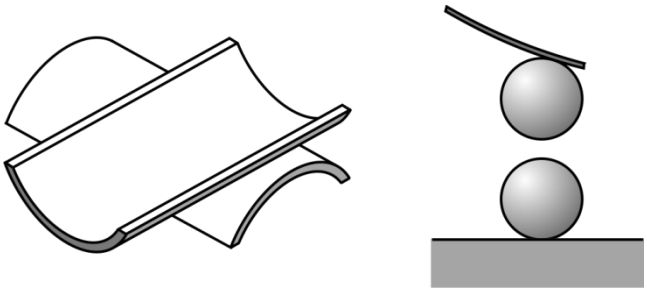

Keywords

Atomic force microscope, AFM, colloidal probe, surface forces apparatus, SFA, double layer forces, van der Waals forces, charge regulation, DLVO theory, non-DLVO forces

1. Introduction

The importance of forces acting between solid surfaces was already pointed out long time ago. In particular, Derjaguin, Landau, Verwey, and Overbeek (DLVO) have recognized that the stability of colloidal suspensions in aqueous electrolyte solutions is governed by the interplay between attractive van der Waals forces and repulsive double layer forces acting between the particles involved [1,2]. While colloidal stability probably represents the prime example, where such forces are of importance, these forces are also essential in many other contexts. For example, they are also relevant in particle deposition to water-solid interfaces, structuring of colloidal suspensions, formation of colloidal crystals and glasses, and sedimentation in particle suspensions [3,4]. To understand such phenomena, knowledge of forces acting between the colloidal particles and interfaces involved is primordial.

In this field, theory largely preceded the experiment. The existence of attractive interactions between molecules was already recognized by van der Waals more than a century ago. Subsequently, the distance dependence of these forces was established and it was further realized that they lead to interactions between macroscopic bodies. These forces were initially assumed to be pair-wise additive, and their relation to dielectric spectra of the materials and to retardation effects due to the finite velocity of light were addressed in the following [3-6]. The electrical double layer forming near a charged interface in electrolyte solutions was known since the early work of Gouy, Chapman, Debye, and Hückel, but the fact that overlapping double layers lead to repulsive forces was only recognized later on [3,7,8]. These developments were refined more recently by including effects of charge regulation, ionic size, polarization, and ion-ion correlations [9-14].

While DLVO theory assumes that interactions can be well approximated by simple superposition of van der Waals and double layer forces, researchers have also investigated other types of interactions, commonly referred to as non-DLVO forces [5]. An important force of this kind is induced by structuring of the solvent near interfaces. This force can be repulsive or attractive, and is also referred to as hydration or hydrophobic interaction, respectively [15-17]. Another type of non-DLVO force is caused by surface charge heterogeneities, which are suspected to induce an additional attraction [18,19]. The existence of longer ranged repulsive non-DLVO forces in concentrated electrolyte solutions was established more recently [20-22].

The possibility to reliably measure forces acing between water-solid interfaces represents a relatively recent development. While early efforts can be traced back to Overbeek, Derjaguin and coworkers [23,24], the breakthrough came around 1970 with the development of the surface forces apparatus (SFA) [25-27]. This technique enabled accurate and reliable force measurements acting between two mica sheets. As time progressed, other techniques for direct force measurements were developed, in particular, the colloidal probe technique based on the atomic force microscope (AFM) [28,29], total internal reflection microscopy (TIRM) [30-32], and optical tweezers coupled to video microscopy [33-35]. With these techniques, measurements of forces involving individual colloidal particles have become routine.

The present article reviews the current state of direct force measurements and the comparison between experimental force profiles with theory. As will be demonstrated, the DLVO framework remains extremely reliable in a wide range of conditions, including interactions between similar as well as dissimilar surfaces. Clearly, this theory has its limitations, and the existence of non-DLVO forces will become apparent as well. To pinpoint the precise origin of those still represents considerable challenges, but guidelines concerning these developments will be given too.

This review addresses forces between solid substrates across aqueous electrolyte solutions. The discussion mainly focuses on symmetric systems, meaning that interactions between identical (or very similar) surfaces are being probed. We also summarize findings in asymmetric systems, meaning that interactions between different (or dissimilar) surfaces are being probed. We shall further argue why proper interpretation of the latter experiments requires simultaneous investigations of the corresponding symmetric systems. Forces between deformable substrates, in other types of liquids, or in aqueous media containing objects of higher molecular mass will not be considered. Concerning these topics, the reader is referred to recent articles and reviews [20,36-40].

2. Derjaguin approximation

Before we address common experimental techniques for direct force measurements, it is helpful to recall the Derjaguin approximation. This approximation relates the force F acting between two curved objects to the surface interaction energy W between two planar walls made of the same material and with the same surface properties. This relation is simple and reads [3,5,41,42]

$$F = 2\pi R_{\text{eff}} W \tag{1}$$

where R_{eff} is the effective radius, which depends on the geometry. For two perpendicularly crossed cylinders of radius R_1 and R_2 as used in the SFA one has $R_{\text{eff}} = (R_1 R_2)^{1/2}$. For two spheres of radius R_1 and R_2 the result is $R_{\text{eff}} = R_1 R_2 / (R_1 + R_2)$. The latter result also includes the case sphere-plane geometry in the limit of one infinite radius, as often used with the AFM. This approximation implies that the measured force can also be reported as the interaction energy W, or equivalently the normalized force F / R_{eff}.

This approximation is only valid when the effective radius is substantially larger than the range of the forces considered. In other words, this approximation applies when the separation distance is small with respect to the size of the object. As forces in aqueous solutions hardly extend further than few tens of nm, the Derjaguin approximation is well satisfied in most geometries used in direct force measurements, with the exception of a sharp AFM-tip.

3. Experimental techniques

Various techniques are currently available to measure forces in various geometries, in particular, between two surfaces, two colloidal particles, or a colloidal particle and a surface. The most important ones include the surface forces apparatus (SFA) [25-27], the colloidal probe technique based on the AFM [28,29], total internal reflection microscopy (TIRM) [30-32] and the optical tweezers techniques combined with video microscopy [33-35]. Let us briefly summarize the possibilities currently offered by these techniques. Figure 1 illustrates their functioning schematically.

Classical SFA measures the interaction between curved mica sheets, which are perpendicularly oriented [5,27]. One sheet is firmly attached next to a microscope objective and the other to a spring. The latter can be moved with micrometer screws and a piezoelectric tube. The measurement proceeds through a precise separation distance determination by means of multiple-beam interferometry. The respective fringes of equal chromatic order are generated by white-light illumination of the mica

sheets, which are coated with a silver layer on their back and observed in transmission through a spectrometer. From the position of these fringes the absolute distance can be determined, while their shape provides information concerning the curvature radius and eventual deformation of these surfaces. The forces are then obtained with the known spring constant from the difference between the actual distance and the piezo motion. The SFA has an excellent distance resolution better than 0.1 nm. While the force resolution of about 10 nN is modest, large curvature radius of the mica sheets, which is on the order of few centimeters, permits the measurement of normalized forces F / R_{eff} down to few μN/m. A recent modification of the SFA opens the possibility to study non-transparent substrates by means of light reflection [43,44]. One can further use the SFA together with metal electrodes, whereby their electric potential can be controlled by means of a potentiostat [44-48]. Further interesting developments include lateral force measurements [49] and high-speed video acquisition [27,50].

The AFM becomes a powerful tool for direct force measurement by replacing the sharp tip with a colloidal probe [28,29]. Such a colloidal probe is obtained by gluing a colloidal particle, typically few μm in diameter, to a tip-less cantilever. By measuring the deflection of this probe in repeated approach and retraction cycles with respect to a substrate, one can measure the force acting between the particle and the substrate. The separation distance can be obtained from the displacement of the piezoelectric material, whereby the contact point can be estimated from the onset of the constant compliance region. Currently, this technique permits measurements down to separation distances of fractions of nm and of forces down to few pN. Since one normally uses particles of few micrometers in diameter, these forces correspond to formalized forces somewhat below 1 μN/m, which is comparable to the SFA. The advantages of the technique are the substantial range of forces and distances accessible, but also the possibility to investigate different geometries and different types of materials. While many researchers work with the classical sphere-plane geometry, one can also use pairs of similar or dissimilar particles [51,52]. The latter measurements require the attachment of the particles to a substrate and vertical centering of the two particles. While this centering could be achieved with the AFM alone, it is easier to use an inverted optical microscope, which is now commonly integrated in an AFM setup. Recent developments involve force measurements with oscillating cantilevers [53] and the use of specially designed cantilevers, which permit aspiration of small colloidal particles by means of nanofluidic techniques [54]. A planar metal substrate under potentiostatic control has also been studied with the colloidal probe [55-57]. One can also perform force measurements with the AFM by means of a sharp tip [58-60]. This approach allows to measure forces at smaller separations, but at the expense of less-defined measurement geometry.

Forces between a colloidal particle and a substrate can also be measured with total internal reflection microscopy (TIRM) [30-32,61]. The technique is based on an evanescent wave generated on a transparent substrate by the total internal reflection of an intense laser beam. The scattered light from a levitating micrometer sized colloidal particle is then collected by means of an optical microscope. The scattering intensity from this particle fluctuates in time due to the thermal motion of the particle, and based on this information the particle-substrate interaction profile can be extracted. One can achieve an excellent distance and force resolution down to few nm and well in the fN regime, which corresponds to normalized forces of 0.1 μN/m. A drawback of TIRM for force measurements is, however, that one can only study sufficiently repulsive particle-substrate interactions, which induce levitation of the particle above the surface.

The optical tweezers technique also offers the advantage that particles can be probed in situ, and there is no need of gluing or attaching the particles to substrates [33-35]. Moreover, forces acting between pairs of colloidal particles can be probed. The technique relies on trapping colloidal particles in a

focused laser beam and measuring their position with video microscopy. The trap acts like a soft spring between the particle and the focal point of the laser, and the respective spring constant can be measured through the thermal fluctuations of the trapped particle, similarly to TIRM [35]. The position of the particle can be determined by locating the center of the intensity distribution of the digital particle image [33]. The precise position of the particle center has to be tracked in time, which becomes progressively difficult when the particles are close to contact [62]. The interaction potential can be deduced from the trajectories of pairs of particles, which were initially positioned with optical traps. Another possibility is to immobilize one particle with a microsyringe and measure the interaction potential with another particle in an optical trap [34]. While the advantage of these techniques is that the force resolution is well below the pN regime, the accessible force range is modest. The distance resolution is normally several nm only, as it is limited by the accuracy by which the particles can be centered. Nevertheless, the future potential of such optical tweezers techniques is substantial.

Addressing surface roughness represents an essential part in most direct force measurements, possibly with the exception of SFA. The latter technique normally uses freshly cleaved mica sheets as substrates, which have been shown to be atomically smooth [60,63]. Most other substrates have an uneven surface topography, especially silica and latex [64,65]. An essential characteristic of such topographic roughness is its root-mean square (RMS), which can be measured by AFM imaging. While roughness influences interaction forces only weakly at distances that are large in comparison with the RMS, it can become important at smaller distances. In these situations, roughness effects can be reduced by means of a sharp tip.

Force experiments are often performed in the asymmetric setting, meaning that the two interacting substrates are made of different materials and/or have different surface properties. This setting is obviously required, when one would like to study interactions between two different substrates. In many situations, however, one is interested to study a symmetric system, whereby the two surfaces should be identical. This situation can be realized with the SFA, when forces between two mica sheets are being probed. A symmetric situation can be also realized with the AFM-based colloidal probe technique or with optical tweezers, when forces between two similar particles are being measured. Due to existing surface heterogeneities, however, the appropriate particle pair must be chosen carefully. In other situations, a symmetric system represents an idealization. The classical sphere-plate geometry used with the colloidal probe or in TIRM measurements is intrinsically asymmetric. The geometry involving an AFM-tip and a flat substrate is also asymmetric. To approximate a symmetric system, one normally chooses the same type substrates on both sides (e.g., silica). Such a system is probably approximately symmetric, but it is nontrivial to establish how symmetric it actually is.

In the following, we will first focus on measurements between mica surfaces with the SFA and between similar colloidal particles with the AFM. In all these situations, the symmetry of the system is satisfied to a good degree of approximation. Further below, we will also address asymmetric systems and demonstrate that a proper interpretation of these systems requires measurements of the corresponding symmetric systems too.

4. Van der Waals Forces

Let us start with symmetric systems and the omnipresent van der Waals force. This force arises from the attraction between permanent and induced dipoles within the materials. In contrast to measurements in air, in aqueous solutions these forces are relatively weak and reliable measurements

were realized only recently. Some examples are summarized in Fig. 2. These experiments were carried out at high salt concentrations (typically >0.1 M) and it was found that this force does not depend on the type of salt used. The observed profiles can be well fitted with the simple relation [3,5]

$$\frac{F_{\mathrm{vdW}}}{R_{\mathrm{eff}}} = -\frac{H}{6h^2} \tag{2}$$

where h is the smallest surface separation and H the Hamaker constant. The latter parameter reflects the strength of the van der Waals force, which is a property of the materials involved. The above equation represents the non-retarded version of the theory, which neglects that interactions can only propagate with the finite speed of light. When such retardation effects are included, they lead to a more pronounced decrease of the van der Waals force with distance. This decrease is often included as a separation-dependent Hamaker constant [6]. In most cases, however, retardation effects across water are small. A minor decrease of the Hamaker constant would be also expected in highly concentrated salt solutions, but these effects are hardly measurable for concentrations ≤ 1 M.

By fitting the measured force profiles with eq. (2) one finds the Hamaker constants of 1.7×10^{-21} J for silica [64,66,67], of 3.3×10^{-21} J for polystyrene [68,69], and 7.8×10^{-21} J for mica [70]. Note that the latter value is markedly lower than the frequently cited value of 2.2×10^{-20} J, which was measured for mica earlier [71]. The values for silica and polystyrene compare well with respective theoretical values [65,72]. However, the measured Hamaker constants for mica are substantially larger than the theoretical estimate of 2.9×10^{-21} J [72]. The mentioned theoretical values are based on the Lifshitz theory, which relies on the dielectric spectra of the materials involved [3,72]. Earlier calculations for mica and silica, which used simplified spectral data, lead to substantially larger values of the Hamaker constants [72]. The theoretical value for polystyrene latex particles further includes effects of surface roughness, which lead to a reduction of the Hamaker constant with respect to smooth surfaces [65]. Such effects are well studied for silica particles, whereby their degree of roughness could be systematically varied [64]. But for the silica substrates discussed here, roughness effects are minor. Roughness effects were also reported to influence van der Waals forces between hafnia surfaces [73]. No roughness effects are expected for atomically flat mica as used in the SFA.

5. Double layer forces and superposition approximation

At lower salt concentrations, double-layer forces become important. DLVO theory suggests that the overall force can be represented by means of two additive contributions, namely [3,5]

$$F = F_{\mathrm{vdW}} + F_{\mathrm{dl}} \tag{3}$$

where F_{vdW} are the van der Waals and F_{dl} double layer interactions. The simplest approximation of the double layer force in a symmetric system is provided by the Debye-Hückel (DH) theory. At large separations, the result reads [3,5]

$$\frac{F_{\mathrm{dl}}}{R_{\mathrm{eff}}} = 4\pi\varepsilon_0\varepsilon\kappa_{\mathrm{eff}}\psi_{\mathrm{eff}}^2\, e^{-\kappa_{\mathrm{eff}}h} \tag{4}$$

where the surface is characterized by a single parameter, namely the effective potential ψ_{eff}, while the bulk electrolyte is described by an effective decay parameter κ_{eff}. The symbol denotes ε_0 the dielectric permittivity of vacuum and ε the dielectric constant of water. This relation can be obtained by superposing the electric potentials generated by the diffuse layers of the two the isolated surfaces, which can be estimated by DH theory. For this reason, we shall refer to eq. (4) as the DH superposition approximation.

Examples of interaction forces involving double layer and van der Waals forces are shown in Fig. 3. We compare interaction energies between silica particles in KCl and $MgSO_4$ solutions, and silica and polystyrene latex particles in KCl solutions. Qualitatively, the data are very similar for all three systems. At low salt concentrations, the forces are repulsive and long ranged. As the salt concentration is being increased, the range and strength of these forces decreases and attractive van der Waals forces start to dominate the system.

At low salt concentrations, forces decay in an exponential fashion, as evident through the appearance of a straight line in the semi-logarithmic representation (Fig. 3, right). The measured data can be indeed well described by adding the double layer force given by eq. (4) and the van der Waals force in eq. (2), as suggested by DLVO theory. This approach introduces two additional parameters, namely the effective potential ψ_{eff} and the effective decay parameter κ_{eff}. The Hamaker constant *H* also enters this description, but its value can be found from force measurements carried out at high salt concentrations.

The experimentally determined effective decay parameter κ_{eff} should be compared with the inverse Debye length κ_{D}. The latter parameter is given by the relation [3,5]

$$\kappa_{\text{D}}^2 = \frac{2q^2 I}{\varepsilon_0 \varepsilon N_{\text{A}} kT} \tag{5}$$

where *q* is the elementary charge, N_{A} is the Avogadro number, *T* the absolute temperature, *k* the Boltzmann constant, and *I* is the ionic strength given by

$$I = \frac{1}{2}\sum_i z_i^2 c_i \tag{6}$$

where c_i and z_i are the molar concentration and valence of the ion of type *i*, and the sum runs over all ions present ion solution. One typically calculates the ionic strength assuming that salts are fully dissociated, whereby we refer to the nominal ionic strength.

The measured decay lengths are plotted versus the nominal ionic strength in Fig. 4. For 1:1 electrolytes, the effective decay parameter κ_{eff} agrees with the inverse Debye length κ_{D} within experimental error. However, major deviations occur for symmetrical electrolytes of higher valence, while minor deviations manifest themselves for asymmetric 1:*z* and *z*:1 electrolytes in the presence of ions of higher valence.

The principal reason for deviations between κ_{eff} and κ_{D} is the formation of ion pairs in solution. While κ_{D} is normally calculated by employing the nominal ionic concentrations, κ_{eff} must be obtained

with the same expression as given in eq. (5), but the ionic strength must be calculated with the appropriate concentrations of the actual ionic species in solution. For symmetric electrolytes, these concentrations can be estimated by considering the chemical equilibrium [74]

$$M^{z+} + X^{z-} \rightleftharpoons MX \tag{7}$$

where M^{z+} and X^{z-} are the cation and anion of valence z, and MX is the neutral ion pair. The concentrations of the free ions can be calculated as a function of the total salt concentration and the equilibrium constant of the ion pairing equilibrium given in eq. (7). Solid lines shown in Fig. 4a are calculations based on this equilibrium. The fitted equilibrium constants agree well with independent measurements of these constants by electric conductivity, dielectric spectroscopy, or ultrasonic absorption [66].

Concerning asymmetric 1:z and z:1 electrolytes, ion pair formation appears negligible in asymmetric 2:1 and 1:2 electrolytes, and the measured decay length agree well with the calculated Debye lengths [61,75]. When considering complexation in solution, one can also well rationalize the observed decay length in solutions of weak acids and bases [69,76,77]. Complex formation is probably also the reason for the minor deviations between observed decay lengths and the calculated Debye length from the nominal ionic strength for ions of valence three, in particular, in solutions of $LaCl_3$ and $K_3Fe(CN)_6$ [75,78].

Let us now focus on the surface potentials and the corresponding surface charge densities. From the magnitude of the double layer force, one can extract the effective potential ψ_{eff} with eq. (4). Since this quantity appears squared, the sign of this potential remains unknown. While all force measurements in symmetric systems suffer from this weakness, the sign of this potential can be determined in various other ways. For many systems, the sign of the potential can be extracted from elecrokinetic measurements (e.g., electrophoresis, streaming potential) [75,79]. The sign can be also inferred from the chemical nature of the surface groups. For example, dissociated silanol and sulfate groups are negatively charged, while amidine groups are positively charged.

For weakly charged surfaces, the effective potential ψ_{eff} corresponds directly to the commonly used diffuse layer potential ψ_{dl}. For more highly charged surfaces, the Poisson-Boltzmann (PB) theory must be used. In this situation, the effective potential ψ_{eff} characterizes the exponential long-distance decay as given by eq. (4), while ψ_{dl} corresponds to the potential at the origin of the diffuse layer. For symmetric z:z electrolytes, these two potentials are related as follows [3]

$$\psi_{\text{eff}} = \frac{4kT}{zq} \tanh\left(\frac{zq\psi_{\text{dl}}}{4kT} \right) \tag{8}$$

This relation can be inverted to extract the diffuse layer potential from the measured effective potential, which can be obtained by fitting eq. (4) to the experimental force profiles. For asymmetric electrolytes, no simple analytic expression is available, and this conversion must be carried out numerically. Alternatively, force profiles can be directly fitted with PB theory.

The interface can be also characterized by means of a surface charge density. An effective surface charge density can be introduced by means of the DH relation [3]

$$\sigma_{\text{eff}} = \varepsilon_0 \varepsilon \kappa_{\text{eff}} \psi_{\text{eff}} \tag{9}$$

The effective potential ψ_{eff} or the effective surface charge density σ_{eff} represent an equivalent way to quantify the charging state of an interface. For sufficiently weakly charged surfaces, the effective charge density reflects the charge needed to neutralize the charge of the diffuse layer. At higher potentials, the PB model must be invoked again. For a symmetric *z*:*z* electrolyte, the simplest way is to insert the diffuse layer potential ψ_{dl} obtained from eq. (8) into the respective charge-potential relationship, which is also referred to as the Grahame equation [3]

$$\sigma = \frac{2kT\varepsilon_0 \varepsilon \kappa_{\text{eff}}}{zq} \sinh\left(\frac{zq\psi_{\text{dl}}}{2kT}\right) \tag{10}$$

The resulting charge density σ represents an equivalent way to characterize the charging state of the diffuse layer. Note that this surface charge neutralizes the so-called diffuse layer charge, which corresponds to the surface charge of the diffuse layer. For asymmetric electrolytes, the corresponding charge-potential relationship must be used [80].

Figure 5 compares the respective diffuse layer potentials and charge densities for various negatively charged interfaces. While a constant charge density reproduces the observed dependence reasonably well, this assumption of constancy is not quite correct. When the inner layer charge density is calculated with eq. (10), one observes that this charge typically decreases with increasing electrolyte concentration. This decrease is especially pronounced in monovalent electrolytes, and could be due to adsorption of anions, ionization of surface groups, or dissociation of adsorbed water molecules. In the presence of multivalent cations, however, this charge density increases. This increase is caused by the adsorption of multivalent cations to the oppositely charged interface.

6. Diffuse and inner layer

It is instructive to compare the observed diffuse layer potentials and surface charge densities with the ones obtained by other techniques. In particular, the surface potential of the bare silica-water interface was recently measured with photoelectron spectroscopy [81]. The surface charge densities of the bare interface can be obtained from potentiometric titrations [82,83]. One finds, perhaps surprisingly, that the values corresponding to the bare interface exceed the values obtained by direct force measurements by about a factor of 10.

To understand this substantial difference, one must consider the structure of the interface in more detail. A scheme is given in Fig. 6. The aqueous side of the interface consists of two sub-layers, namely the diffuse and the inner layer. The diffuse layer may extend far into the solution. As in this layer the respective ionic concentrations and electric potential are low and vary gradually. These profiles structure can described with the PB model. However, ions also bind to surface groups tightly, and they form a dense and thin layer within about the last nm of the interface. The ionic concentrations in this compact layer are high and the electric potential decays rapidly. We will refer to this part of the interface as the inner layer. Protons (or other ions) will bind in a specific fashion to the surface groups, or they may form a compact layer close to the solid interface, and thus contribute to the surface charge. Numerous authors developed detailed surface complexation models involving various additional sub-layers (e.g., Helmholz layer, Stern layer) to describe these effects [82,84-87]. Besides specific ion-

surface interactions, however, packing and ion-ion correlations are also important in the inner layer [88,89]. For this reason, the proper description of the inner layer remains a challenge.

The substantial difference between the electric potentials and the respective charge densities results from a near-complete neutralization of the surface charge of the bare interface by adsorbed counterions in the inner layer. Only a small fraction of the surface charge is neutralized within the diffuse layer, and this remaining charge is the one that is measured in the direct force experiment. We note that the present scenario refers only to moderately strongly adsorbing ions. When very strongly adsorbing counter ions are involved, the charge accumulated in the inner layer may exceed the one of the bare interface. This situation leads to charge reversal, and this phenomenon will be further discussed in Sect. 9.

7. Beyond superposition approximation

While the simple DH superposition approximation leading to the exponential profile given by eq. (4) is only rigorously valid at sufficiently large separation distances, often it works even down to rather small separations. Such situations are quite frequent, and typical examples were illustrated in Fig. 3.

In some cases, however, the DH superposition approximation can become poor even at relatively large distances. The most important case is surely the symmetric situation in electrolyte solutions involving multivalent co-ions [90]. Recall that multivalent co-ions have the same sign of charge as the surface. Force measurements between negatively charged sulfate latex particles in 1:1, 1:2, 1:3, and 1:4 electrolytes at a common ionic strength of 1.0 mM illustrate this situation, see Fig. 7a. In the 1:1 electrolyte, the simple exponential law is valid down to nm-distances. As the valence of the co-ion increases, one observes that the exponential law sets in only at increasingly larger distances, for the 1:4 electrolyte even beyond 50 nm. In the semi-logarithmic representation, the force profiles show a characteristic sigmoidal shape, which is well described by the PB model. The PB model is also capable to rationalize the concentration dependence of this profile, as illustrated in Fig. 7b with the 1:4 electrolyte. The range of the double layer force decreases with increasing concentration, but its sigmoidal shape is maintained.

The reason why the DH superposition approximation is poor for multivalent coions is that these ions are expelled from the vicinity of the like-charged surface, and a surface layer free of co-ions is formed. While such a layer also forms in 1:1 electrolytes, it remains thin, but its thickness increases rapidly with the valence of the co-ions. At smaller distances, the surfaces interact across a layer containing counter-ions only, and in this situation the forces follow a slowly decaying power law. The crossover from this power-law at short distances to the exponential decay at larger distances leads to the characteristic sigmoidal shape of these force profiles.

8. Charge regulation

The DH superposition approximation may also fail in symmetric systems due to charge regulation effects [9,91-93]. As charged surfaces approach, they regulate their surface charge. The extent of charge regulation is determined by interplay between the charging of the inner layer and of the diffuse layer upon approach. One possibility to address this interplay involves surface complexation models [9,92,94,95]. Such models describe the adsorption equilibrium with appropriate mass action laws that

are coupled to corresponding surface potentials. In the simplest case, the charging of an interface by protons can be described with a single adsorption reaction [82,84,92]. Regulation of the surface charge upon approach can be predicted with such models. The disadvantage of such surface complexation models is that they often involve numerous adjustable parameters, which cannot be simply extracted from measured force profiles.

The constant regulation (CR) approximation provides an alternative approach, which permits to describe the regulation behavior with a single regulation parameter p [91-93]. When the surface charge remains constant upon approach, one refers to constant charge (CC) conditions, and one has $p = 1$. The diffuse layer potential may also remain constant upon approach, whereby one refers to constant potential (CP) conditions and $p = 0$. While the regulation parameter may assume any value $p \leq 1$, in practice one finds values between the CP and CC situations. The CR approximation can be shown to be asymptotically correct at larger distances. The corresponding regulation parameters can be also extracted from the respective surface complexation models [92,96].

The DH model allows evaluating forces within the CR model explicitly. The resulting expression reads [91,93]

$$\frac{F_{\mathrm{dl}}}{R_{\mathrm{eff}}} = 4\pi\varepsilon_0\varepsilon\kappa_{\mathrm{eff}}\psi_{\mathrm{eff}}^2 \frac{e^{-\kappa_{\mathrm{eff}}h}}{1+(1-2p)e^{-\kappa_{\mathrm{eff}}h}} \tag{11}$$

At larger distances, the force profiles always converge to the common exponential dependence given by the DH superposition approximation, irrespective of the regulation conditions used. One observes that the forces becomes more repulsive for the CC conditions, and more generally for $p > 0.5$, while they are less repulsive for the CP conditions and $p < 0.5$. In practical situations, however, the diffuse layer potentials in question are often beyond the validity of the DH model. For this reason, it is preferable to use a numerical solution of the PB model, which includes the CR approximation, for comparison with experimental data. Comparison of such PB calculations involving the CR approximation with calculations based on explicit surface complexation models demonstrates that the CR can be surprisingly accurate down to very small distances [92,96].

Figure 8 illustrates charge regulation effects with force measurements between negatively charged silica particles in various 1:1 electrolyte solutions. DLVO theory including van der Waals forces and the PB model with CR conditions was used to obtain the calculated curves. We always show the best fit with the CR conditions, together with the CC ($p = 1$) and CP ($p = 0$) conditions for comparison. For the CsCl electrolyte and pH 4, the regulation parameter $p = 0.45$ is intermediate between the CP and CC cases. For the LiCl electrolyte at the same conditions, one finds $p = 0.69$, and thus the surface regulates its charge less easily. When one considers the CsCl electrolyte again, but now at pH 10, the force profile is with $p = 0.91$ close to the CC condition. When these calculations are compared with the DH superposition approximation, one observes that this model is very good for the data shown in in Fig. 8a, while it fails substantially for those shown in Fig. 8c. One can understand this behavior by comparing eqs. (4) and (11). In fact, the superposition approximation is exact for $p = 0.5$, while it progressively worsens near the CC and CP situations.

The regulation parameter varies systematically with the type of electrolyte and pH. These results are summarized in Fig. 9a. The regulation parameter systematically decreases in the series Li^+, Na^+, K^+,

and Cs^+. At pH 4, one observes a weak increase with increasing concentration, while at pH 10 a marked decrease.

To interpret these trends, let us recall the structure of the interface involving the inner layer and the diffuse layer, as shown in Fig. 6. Charge regulation reflects the different charging characteristics of these two layers. These characteristics can be quantified in terms of capacitances, namely C_{dl} for the diffuse and C_{in} for inner layer. The diffuse layer capacitance can be obtained from the derivative of eq. (10), and reads

$$C_{\mathrm{dl}} = \varepsilon_0 \varepsilon \kappa_{\mathrm{eff}} \cosh\left(\frac{zq\psi_{\mathrm{dl}}}{2kT}\right) \tag{12}$$

The inner layer capacitance reflects the charging behavior of the inner layer and can be thought of as the capacitance of the Stern layer to a first approximation. Within this picture, the regulation parameter reads [91-93]

$$p = \frac{C_{\mathrm{dl}}}{C_{\mathrm{dl}} + C_{\mathrm{in}}} \tag{13}$$

Based on eqs. (12) and (13) together with the measured diffuse layer potentials, one can evaluate the inner layer capacitance. These results are shown in Fig. 9b. One observes that this capacitance increases with concentration, modestly at pH 4 and very strongly at pH 10. This increase reflects that this capacitance is not simply constant, as the notion of a Stern capacitance might suggest. We suspect that this dependence originates from variations in the adsorbed amount of salt ions. One further finds that the inner layer capacitance increases in the series Li^+, Na^+, K^+, and Cs^+. These variations probably reflect changes of the dielectric constant in the proximity of the interface [97]. Very similar values and trends were obtained by extracting Stern capacitances from X-ray photon spectroscopy, electrophoresis, and titration data [81,83]. At this point, however, an interpretation of these trends with more microscopic models of the inner layer is lacking. Further details concerning charge regulation effects can be found in a recent review article [93].

Another important observation is that charge regulation characteristics of close to neutral surfaces can be often approximated with CP conditions [69,98]. This feature can be easily understood based on eqs. (12) and (13). For an uncharged interface, the diffuse layer potential is small, which leads to a small diffuse layer capacitance. When this capacitance is small, the regulation parameter will be close to zero.

9. Charge reversal

So far we have discussed symmetric systems and the classical screening scenario, which implies that the surface charge density remains roughly constant as the salt concentration is being increased. In this situation, forces are dominated by repulsive double layer forces at low concentrations and by attractive van der Waals forces at high concentrations. Let us now focus on the second scenario, which is relevant for symmetric systems. Thereby, counter-ions adsorb so strongly that they induce a charge reversal of the substrate. A charge reversal is normally observed when changing the concentration of strongly adsorbing counterions [46,68,69,75,99] or by pH variations for metal oxides [73].

Experimental force profiles typical for this situation are shown in Fig. 10. Let us first focus on the situation shown in Fig. 10a, where the charge reversal is induced by a polyamine denoted as N6 [69]. The caption of Fig. 2 provides further details on N6. About four of the six amine groups of this polyamine are protonated under the conditions investigated. This species adsorbs strongly to the negatively charged sulfate latex particles, and induces a charge reversal. As the concentration is increased, this reversal manifests itself as a decrease of the magnitude of the double layer repulsion, followed by a reentrant increase. Thereby, the range of the interaction remains approximately constant. At charge neutralization, which is induced at 11 μM, the force is attractive. The existence of the charge reversal was further confirmed with electrophoresis experiments. At higher salt concentrations, the screening scenario discussed above set in. A similar reentrant situation can be observed for monovalent tetraphenyl arsonium ions, denoted as Ph_4As^+ [68]. The respective data are shown in Fig. 10b. While these ions are monovalent, they adsorb strongly again due to their substantial hydrophobicity, thereby inducing a charge reversal.

The observed force profiles can be rationalized with DLVO theory with the PB model and CR approximation. The Hamaker constant was adjusted by means of measurements at high salt concentrations. A similar description can be also achieved with the DH superposition approximation, but in both situations the systems regulate their charge strongly, and this situation is best captured with PB theory including CR approximation. The diffuse layer potential must be extracted from the fits. These potentials together with the corresponding surface charge density are shown in Fig. 11a. Both quantities indicate the charge reversal clearly. One notes that the charge density increases substantially beyond the change reversal point, which confirms that the counterions continue to adsorb. A very similar charge reversal was observed in other systems, for example, for silica in the presence of hydrophobic monovalent cations, or for positively charge amidine latex particles and multivalent anions [69,75]. A charge reversal was also found with the SFA for gold surfaces under potentiostatic control in the presence with perchlorate ions [46], and for mica surfaces in the presence of divalent counterions, but at rather high electrolyte concentrations [99].

The characteristic aspect of the charge reversal scenario is that the range of the reentrant double layer force remains approximately constant, since the salt concentration does not vary substantially near the charge reversal point. On the contrary, in the screening scenario, the range of the double layer force decreases substantially with increasing concentration, before it becomes attractive. Another characteristic feature of the force profiles shown in Fig. 10 is that the measured force profiles are more attractive than predicted with DLVO theory. This additional non-DLVO attraction will be discussed in the following.

10. Attractive non-DLVO forces

Numerous authors have studied symmetric systems and reported additional attractive forces, which cannot be rationalized with the classical DLVO theory. An early example of attractive non-DLVO forces was observed for mica sheets in solutions cetyltrimethylammonium bromide (CTAB) [17]. This force was found to be consistent with an exponential law, namely

$$\frac{F}{R_{\text{eff}}} = Ae^{-qh} \tag{14}$$

where q^{-1} is the decay length and A its amplitude with $A < 0$. The decay length was found about 1 nm and magnitude of the amplitude about 100 mN/m. This force was originally interpreted as hydrophobic interaction originating from the structuring of water near a hydrophobic interface.

Since this early study, one could witness substantial research activity to establish the nature of these interactions more precisely. However, many of these results were conflicting, especially since much more long-ranged forces were reported [15,16,100,101]. Such long-ranged forces cannot be explained by solvent structuring, since its decay length should be comparable to the size of the water molecule. Short ranged attractive forces have been observed as well, especially for hydrophobic substrates, where the decay length is clearly below 1 nm [15,16,98,102,103]. These forces could be well compatible with a depletion of the solvent near the surface. Longer-ranged forces, however, cannot be easily reconciled with solvent depletion, unless clusters of several water molecules participate in forming a hydrogen bonding network. While computer simulations recently suggested the possibility of such clusters [104], their existence remains speculative, and it is unclear whether they could induce attractive forces between surfaces.

Alternative explanations of the long-ranged non-DLVO interactions are more likely. An important contribution was the finding that stable nanobubbles may form on hydrophobic surfaces, and bridging of these nanobubbles may induce attractive forces acting over hundreds of nanometers [105,106]. By now, the possibility that such nanobubbles form on hydrophobic substrates is firmly established. Therefore, the presence of such nanobubbles may influence the interaction forces in some situations, but their presence can be largely eliminated by degassing the solutions and proper preparation of the substrates.

More recently, various reports of attractive non-DLVO forces became available, where the presence of nanobubbles could be excluded [68,107-109]. Some of these experiments were carried only in simple salt solutions. In such situations, contributions of DLVO forces must be considered. To exclude double-layer forces, one may work with neutral surfaces. A good way to obtain such a surface is to neutralize the surface charge with an adsorbing counterion.

Examples of forces observed in such experiments are shown in Fig. 12. The neutral surface was obtained by adsorption of hydrophobic ions [68], multivalent metal ions [107], or adsorbed surfactants [108,109]. Similar features are observed in all situations. The attractive forces measured are clearly stronger than the van der Waals force. For the systems shown in Fig. 12a,b the van der Waals force was also measured in the same system at high salt concentration [68,107]. These measurements further demonstrate that these additional forces can be suppressed by addition of salt. Note that in Ref. [68] a plot similar to Fig. 12b was shown (Fig. 5 in that reference), but the y-axis was labeled incorrectly. The correct labeling is now given in Fig. 12. Similar attractive non-DLVO forces were also reported in other systems in the presence of multivalent ions [69,77,78,110-112] and surfactants [100,113].

The observed force profiles can be well rationalized with an attractive exponential interaction given by eq. (14). When the surface charge is neutralized with small molecules, the decay length is in the range of 1–3 nm and the amplitudes normally do not exceed 1 mN/m. For surfactants, the decay lengths are substantially larger, typically 3–30 nm, and the amplitudes increase to 10 mN/m. These decay lengths are too large that they could be explained by water structuring. Moreover, potential structuring effects are hardly compatible with the fact that these forces vanish at high salt [69,77,78,108-113]. The effect of salt on these forces was studied for CTAB [108] and for multivalent metal complex $Co(NH_3)_6^{3+}$

[112]. Both studies demonstrate that the force remains exponential, but that its decay length decreases with the salt level.

This longer-ranged force could originate from a laterally heterogeneous charge distribution on the substrate [18,19,114]. Indeed, analysis of interaction between surfaces with such a patch-charge charge distribution arranged on periodic lattices confirms that at longer distances there is an additional interaction that follows the exponential law given in eq. (14). For a square lattice, the decay length q^{-1} is given by the relation [18]

$$q^2 = \kappa_D^2 + \left(\frac{2\pi}{\ell}\right)^2 \tag{15}$$

where κ_D is the Debye parameter given by eq. (5) and ℓ the lattice spacing. This relation predicts that the decay length is determined by the lattice spacing at low salt levels, and by the Debye length at higher salt levels.

Nevertheless, interactions between patchy surfaces are complex. The interaction is repulsive when the surfaces are locked into register, meaning that equally charged patches face each other upon approach. An attractive interaction is predicted, when the surfaces are locked out of register, meaning that oppositely charged patches face each other upon approach. When the surfaces are free to equilibrate thermally upon approach, the interaction is attractive and the decay parameter can be still obtained by eq. (15), but one must replace q by $2q$, meaning that the decay length is halved. An important situation arises in the case of a random arrangement of the surface charge heterogeneities. When these heterogeneities are weakly charged, one finds a repulsive force for CC boundary conditions [114]. On the other hand, large and highly charged patches induce an overall attraction [19,115].

In spite of these uncertainties, the patch-charge mechanism explains several experimentally observed features. Most importantly, decay lengths much smaller than the Debye length, as exemplified in Figs. 12a,b, could reflect the patch size. Decay lengths close to half Debye length, as illustrated with the CTAB system shown in Fig. 12c, could be caused by thermal equilibration of interactions between larger patches. When the decay length of the attractive force corresponds to the Debye length, as shown in Fig. 12d and reported in Refs. [109,113], this situation could be caused by locked-in patches, which are much larger than the Debye length. The patch-charge mechanism also explains why these forces vanish at high salt. As these forces originate from double layer interactions, they are screened by adding salt. In particular, the decrease of the decay length with increasing salt level can be explained with eq. (15) too.

The existence of such patchy surfaces was confirmed for adsorbed CTAB layer to mica by AFM imaging and X-ray scattering [116]. These surface heterogeneities are probably due to formation of islands of positively charged of CTAB bilayers on a negatively charged mica background. However, patchy structures may reflect inherent surface charge heterogeneities (e.g., polystyrene latex) or inhomogeneties in the adsorbed layers. Such patch-charged surfaces could originate by templating the inhomogeneties of the substrate, or generated within the adsorbed layer through ion-ion correlations or spontaneous charge fluctuations.

Spontaneous charge fluctuations are known to generate attractive non-DLVO forces since the work of Kirkwood and Shumaker [117]. In the plate-plate geometry and large separations, the interaction energy becomes [118-121]

$$\frac{F}{R_{\text{eff}}} = B\frac{e^{-2\kappa_D h}}{h} \tag{16}$$

with $B < 0$. The decay length of the exponential is half the Debye length, which reflects a thermally averaged force between large patches. Due to the additional algebraic decay, this force decays more rapidly with distance than a simple exponential. As shown in Fig. 12c, interactions between adsorbed CTAB layers can also be well fitted when eq. (16) is added to the van der Waals force [108,120]. However, given the noise in the experimental force profiles one cannot reliably distinguish eqs. (14) and (16). One should further note that all other data shown in Fig. 12 are incompatible with eq. (16).

While patch-charge surface heterogeneities are likely to represent the origin of many reported long-ranged attractive non-DLVO forces, this explanation is not applicable to some systems. Especially for highly hydrophobic substrates, long-ranged attractive non-DLVO forces do not always disappear at high salt levels [122,123]. Possibly, these interactions could arise from spontaneous nucleation of nanobubbles between approaching surfaces. Such spontaneous cavitation effects were in fact observed in computer simulations [124].

11. Repulsive non-DLVO forces

In symmetric systems, short-ranged repulsive non-DLVO forces are omnipresent for strongly hydrated and highly charged mineral surfaces, such as mica, silica, and metal oxides [70,78,125-128]. The range of these forces is normally small, typically below one nanometer. This force can be approximated by the exponential law given in eq. (14) with $A > 0$. For smooth substrates, such as mica, or when forces are probed with an AFM tip, oscillatory forces due to structuring of the salt ions or solvent molecules occur in this regime [22,58-60,70,128]. For other substrates, the oscillatory component disappears due to roughness effects and only a monotonic repulsion is being observed. For silica, a hairy layer was further suggested to contribute to the short-ranged repulsive force [126].

A longer-ranged repulsive non-DLVO force has been observed between charged substrates in symmetric systems and concentrated electrolyte solutions, typically at concentrations >1 M [21,22,129]. Illustrative examples are shown in Fig. 13. This force resembles the DH decay, but the decay length is much larger than the Debye length expected from eq. (5). Moreover, volume fraction of the ionic species is >0.1 at these concentrations, meaning that the electrolyte solution is highly concentrated. Under such conditions, the DH theory is expected to be invalid, since this model assumes point-like ions. Similar repulsive and/or oscillatory non-DLVO forces were also reported in ionic liquids [130].

In contrary to what is suggested by DH theory, the observed decay length in fact increases with increasing electrolyte concentration, see Fig. 14a. Such an increase cannot be explained by simple ionic pairing, since as illustrated in Fig. 4, this effect will only cause a weaker decrease of the decay length with the concentration, but not an increase. The observed dependence of the apparent decay length q^{-1} follows the empirical scaling law

$$\frac{q}{\kappa_D} \propto \left(a\kappa_D\right)^{-\nu} \tag{17}$$

where a is the ionic diameter, κ_D is the inverse Debye length given by eq. (5), and the exponent $\nu = 3$. In other words, the decay length increases proportionally to the salt concentration c, namely as $q^{-1} \propto c$. These scaling laws are also indicated in Fig. 14 together with the classical DH dependence given by eq. (5).

While discussion concerning the origin of these forces is currently ongoing, an interesting interpretation is based on an analogy with Schottky defects in ionic crystals. Such neutral defects occurring in ionic crystals interact with Coulomb-like forces, and thus resemble a dilute electrolyte solution. For this reason, in concentrated electrolytes solvent molecules could play a similar role as Schottky defects in ionic crystals.

Based on this analogy, Lee et al. [131] were able to derive the experimentally observed exponent $\nu = 3$ in eq. (17). While a more rigorous analysis based on integral equations and density functional theories suggest similar dependencies, but smaller exponents ν in the range 1.5–2 are found [132,133]. These theoretical treatments further suggest that the force profiles should also include an oscillatory component due to packing effects. Indeed, some experiments confirm the presence of such oscillations [22]. These theories also predict a region where the decay length should be decreasing more rapidly than predicted by the DH theory. This region is not observed in the experiments shown in Fig. 14, but it could be masked by formation of ion pairs or a charge reversal of the mica surface. Such a charge reversal was established in the presence of divalent cations for mica and silica, and in CsCl solutions for silica [99,129]. The decay lengths in this regime are expected to be small, and the measured forces are difficult to disentangle from hydration forces.

12. Asymmetric systems

One can also study two types of surfaces A and B, and the interactions in the system AB. Meaningful experiments with asymmetric systems should be always accompanied with the corresponding experiments in the symmetric system. The ideal situation is to carry out experiments with both corresponding symmetric systems, namely AA and BB. To realize measurements with only one of the symmetric systems, thus either AA or BB, is sufficient. What should be avoided, however, is to study the asymmetric system AB alone.

The necessity to combine symmetric and asymmetric measurements originates from the nature of double layer forces. As these forces are omnipresent, it is natural to strive towards their meaningful interpretation. Within the DH superposition approximation, the double layer force in an asymmetric system decays at large distances as [3]

$$\frac{F_{dl}}{R_{eff}} = 4\pi\varepsilon_0\varepsilon\kappa_{eff}\psi_{eff}^{(A)}\psi_{eff}^{(B)}\, e^{-\kappa_{eff}h} \tag{18}$$

where $\psi_{eff}^{(A)}$ and $\psi_{eff}^{(B)}$ are the effective potentials of the surface A and B. Since these two quantities appear as a product, it is impossible to determine their individual values from the force measurement in the asymmetric system AB alone. However, when one measures the interaction in one of the symmetric systems, say AA, one can extract the effective potential $\psi_{eff}^{(A)}$ for the surface A, see eq. (4). One still has to determine the sign of this potential, but as discussed in Sect. 5, this problem can be normally resolved easily. Once the value of $\psi_{eff}^{(A)}$ is known, the measurement in the asymmetric

system AB can be used to extract the effective potential $\psi_{\mathrm{eff}}^{(\mathrm{B})}$ of the surface B. From this measurement, even the sign of this potential can be determined.

The situation is even more problematic when the full PB model is being used for data interpretation. In this case, one must also consider charge regulation effects, and within the simple constant regulation approximation, two additional regulation parameters must be introduced. When solution concentrations of all ionic species are known, double layer forces in asymmetric setting AB involve four adjustable parameters, namely for each surface the two diffuse layer potentials $\psi_{\mathrm{dl}}^{(\mathrm{A})}$ and $\psi_{\mathrm{dl}}^{(\mathrm{B})}$ and the two regulation parameters $p^{(\mathrm{A})}$ and $p^{(\mathrm{B})}$. Normally it is impossible to reliably extract these four parameters from a single force curve. However, one can extract, say $\psi_{\mathrm{dl}}^{(\mathrm{A})}$ and $p^{(\mathrm{A})}$ from the symmetric setting. Once these parameters are known, they can be fixed for the analysis of the asymmetric case, and the other set of parameters $\psi_{\mathrm{dl}}^{(\mathrm{B})}$ and $p^{(\mathrm{B})}$ can be obtained. Thereby, it is advantageous to choose the more highly charged system for the symmetric setting, and include the more weakly charged surface in the asymmetric one.

This type of analysis is illustrated in Fig. 15. The measurements in symmetric systems are shown in left column of Fig. 15. As discussed above, these profiles can be fitted with PB theory including the CR approximation, whereby one obtains the diffuse layer potential and the regulation parameter for one of the surfaces studied. The asymmetric systems are fitted with the same model, whereby the parameters obtained from the symmetric systems are then fixed. These results are shown in the right column of Fig. 15, and from the fits the respective parameters for the other surface can be extracted.

Note that the experiments shown in Fig. 15a,c were carried out with two different probe particles A and B but the same planar silica substrate C. In both situations AC and BC, the parameters extracted for the silica substrate C are the same, which provides an independent cross-check of the present analysis [134]. Another possibility to perform such a cross-check to study three different particle pairs, namely AA, AB, and BB. This type of consistency analysis was successfully carried out with various latex particles [75,77,98,135].

Figure 15 equally illustrates the main characteristic features of the double layer forces in asymmetric systems. As predicted by eq. (18), the double layer force is attractive for two oppositely charged surfaces, while this force is repulsive for two like-charged surfaces (Fig. 15a,c, right).

When one of the surfaces is neutral, eq. (18) suggests that the double layer force vanishes. However, this conclusion is incorrect, since this relation only reflects the leading large-distance term. In this charge-neutral case, the DH theory predicts the following next order term [91,93]

$$\frac{F_{\mathrm{dl}}}{R_{\mathrm{eff}}} = 4\pi\varepsilon_0\varepsilon\kappa_{\mathrm{eff}}[\psi_{\mathrm{eff}}^{(\mathrm{A})}]^2[1-2p^{(\mathrm{B})}]e^{-2\kappa_{\mathrm{eff}}h} \tag{19}$$

whereby the surface A is charged, while the surface B uncharged ($\psi_{\mathrm{eff}}^{(\mathrm{B})} = 0$). This double layer force has interesting properties. While its dependence is also exponential, the respective decay length is half of the Debye length. The sign of this force depends on the regulation parameter of the neutral surface B. For CC conditions ($p^{(\mathrm{B})} = 1$), this force is repulsive, while for CP conditions, ($p^{(\mathrm{B})} = 0$), it is attractive. This charge-neutral case is also illustrated (Fig. 15b, right). This situation was realized with a highly charged sulfate latex particle and a neutral amidine particle [135]. The measured force is attractive, since the neutral amidine particle surface is close to CP boundary conditions. By

considering the CC and CP conditions, which are also illustrated in the figure, one observes the huge effect of charge regulation in this charge-neutral case.

Consideration of charge regulation is essential to properly interpret such force experiments in the asymmetric setting [93]. This aspect is particularly important, since a similar contribution as given in eq. (19) is present for charged surfaces as well. For this reason, double layer forces may feature maxima or minima, as illustrated on the right hand side of Fig. 15a,c. These features can be properly described only by considering charge regulation effects.

Within the same system, one can realize repulsive as well as attractive double layer forces, when one of the surfaces undergoes a charge reversal, while the other one maintains the same sign of charge. This situation can be achieved, when the solution contains ions that strongly adsorb to the oppositely charged surface, but only weakly to the like-charged one [77,98,136]. Another possibility to realize this situation is to study interactions between a charged surface, such as silica or mica, and a metal surface under potentiostatic control [48,55,56]. Thereby, the charge of the metal surface, which typically is gold, can be tuned by means of an external potentiostat.

Typical force profiles in both situations are illustrated in Fig. 16. These profiles were fitted with the PB model including the CR approximation. Thereby, the corresponding symmetric system was always used to extract the parameters of the highly charged surface, while the respective parameters for the surface undergoing charge reversal were obtained from the asymmetric system.

The left column of Fig. 16 shows situations where the surfaces are oppositely charged, and thereby the leading term given by eq. (18) is attractive. The right column, on the other hand, illustrates situations where these forces are repulsive. Force profiles near the charge neutralization point are shown in Fig. 16, middle. These interaction profiles are again dominated by charge regulation effects. In all situations, the resulting force is attractive suggesting that charge regulation is very prominent, and close to CP conditions. The reason for this behavior can be found in eqs. (12) and (13). When the surface is neutral, the diffuse layer capacitance is small, which leads to a small regulation parameter.

When adsorbing ions induce the charge reversal of one surface, as shown in Fig. 16a,b, this surface features strong charge regulation, often close to CP. For this reason, forces are attractive even in the charge-neutral case. The situation is different for a gold electrode for which the charge reversal is induced by applying an external potential. The data by Hillier et al. [55] shown in Fig. 16c suggest regulation conditions between CC and CP ($p = 0.49$). A similar intermediate regulation conditions were described for thiol-modified gold electrodes [56]. On the other hand, measurements with the SFA involving a mica sheet and a gold electrode undergoing a charge reversal could be reasonably well interpreted with CP conditions for the gold electrode [137]. Clearly, further work is necessary to clarify the regulation characteristics of metal electrodes under potentiostatic control.

Only few reports concerning measurements of van der Waals forces are available for asymmetric systems. One exception concerns force measurements between sulfate and amidine latex particles of different size at high salt concentrations [98]. As expected, the force profiles in symmetric and asymmetric systems are all compatible with single value of the Hamaker constant.

The same study also reports attractive non-DLVO forces in asymmetric systems [98]. While such forces are also found, they are difficult to observe due to the presence of attractive double layer forces. Attractive non-DLVO forces persisting to high salt levels were also observed between surfaces of different hydrophobicity [122].

Exponential non-DLVO forces at high electrolyte concentrations were not reported in asymmetric systems so far. However, similar attractive forces were evidenced to act in ionic liquids between an oppositely charged mica surface and a gold surface under potentiostatic control [138]. This sign reversal confirms the electrostatic character of these forces.

13. Conclusions

We have reviewed the current status of direct force measurements involving two solid bodies in aqueous solutions containing monovalent and multivalent ions. These forces can be interpreted with DLVO theory, which relies on a superposition of van der Waals forces and double layer forces. Van der Waals forces can be well represented with the non-retarded model, while double layer forces with a simple exponential. While the latter can be derived from the DH superposition approximation, the full PB model can be necessary to describe double layer forces in asymmetric electrolytes where the multivalent represent the co-ions or when charge regulation effects become important.

The parameters entering the PB model are effective quantities. To account for the correct screening length of the electrolyte solution, one must consider solution speciation, including formation of ion pairs, solution complexes, or respective ionization equilibria. The strength of the interaction is mainly determined by the diffuse layer potential or the corresponding surface charge density. These quantities are normally substantially smaller in magnitude than the bare surface potential or the bare surface charge, and this reduction is due formation of tightly packed adsorbed layers in the vicinity of the interface. Sometimes, these layers may even induce a charge reversal. The characteristics of the inner layer also determine the charge regulation properties, such as, constant charge, constant potential, or intermediate behavior. The detailed description of this inner layer is difficult, as specific ion adsorption, ion-ion correlations, and hard-core interactions must be considered. Nevertheless, more detailed information concerning the inner layer would be essential, as these insights should enable us to predict the appropriate diffuse layer potentials and the regulation properties from fundamental principles. Most promising in this direction are X-ray and light reflectivity methods that permit to measure ion adsorption processes in situ [139,140], high resolution AFM tools that provide information about the lateral structure of adsorbed layers [60,63,141], and simulation techniques that permit to address its structure [58,140].

Cautionary voices were raised concerning the validity of the PB model in the presence of the multivalent ions [10,11]. However, these authors did not invoke any effective parameters in this model. When the appropriate effective quantities are used, the PB model turns out to be highly accurate at distances beyond few nm [88,89]. However, appropriate schemes to extract such effective quantities are poorly established, and further developments in this direction would be desirable.

While the situation in the symmetric setting is reasonably well established, there are fewer studies involving the asymmetric setting. DLVO theory remains reliable in this situation as well. Since many parameters must be determined, however, it is essential to combine measurements in asymmetric system with measurements of at least one of the symmetric systems. In the asymmetric setting, consideration of charge regulation is essential, especially when one of the surfaces is weakly charged.

Deviations from DLVO theory are observed at small distances, typically below few nm. In some situations, more long-ranged attractive non-DLVO forces are found, especially in the presence of adsorbed molecular layers or for hydrophobic surfaces. The origin of the latter forces still remains a

matter of debate, but the likely origin of these forces is electrostatic attraction between patch-charged surfaces. This patchy structure may originate from charge-fluctuations, heterogeneous charge distributions, or inhomogeneous substrates. In concentrated salt solutions, longer ranged repulsive non-DLVO forces were observed and they were suggested to be related to Schottky defects. Further research is necessary to clarify these questions further.

Acknowledgements

We thank Frieder Mugele for stressing the usefulness of surface charge densities in data interpretation. We also acknowledge useful discussions with David Andelman, Klemen Bohinc, Sven Behrens, Matej Kanduc, Christophe Labbez, Leo Lue, Rudi Podgornik, and Markus Valtiner. This research was supported by the Swiss National Science Foundation and the University of Geneva.

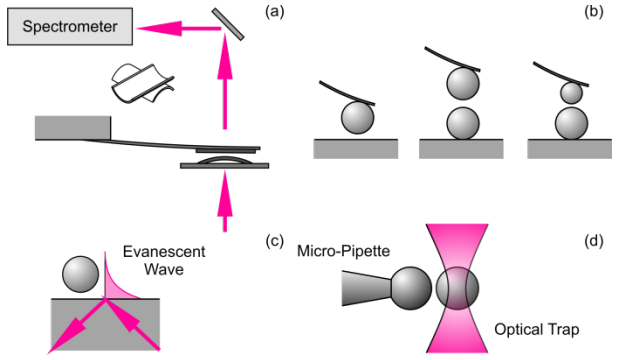

Figure 1. Schematic representation of common techniques for direct force measurements. (a) Surface forces apparatus (SFA) indicating the symmetric crossed-cylinder geometry with two bent mica sheets. (b) Colloidal probe technique based on the atomic force microscope (AFM) in the asymmetric sphere-plane geometry and the symmetrical and asymmetrical sphere-sphere geometry. (c) Total internal reflection microscopy (TIRM) where distance of a levitating particle is being probed with an evanescent field. (d) Optical tweezers technique combined with video microscopy, where one particle is positioned with the trap and the other with a micropipette.

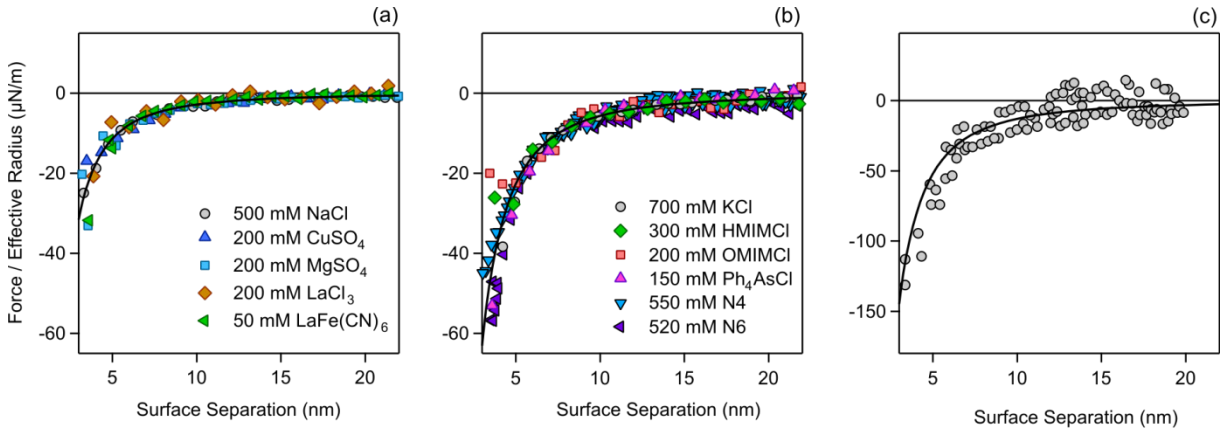

This is a double column figure. Do not print this text.

Figure 2. Measurements of van der Waals forces in concentrated salt solutions. Solid line is the best fit with the non-retarded force law given in eq. (2). Colloidal probe technique was used for (a) silica particles in various inorganic electrolytes [66] and for (b) sulfate latex particles in solutions containing organic ions [68,69]. The abbreviations refer to tetraphenylarsonium chloride (Ph_4AsCl), 1-hexyl-3-methylimidazolium chloride (HMIMCl), 1-octyl-3-methylimidazolium chloride (OMIMCl), triethylenetetramine (N4), and pentaethylenehexamine (N6). The concentrations of the polyamines correspond to the nitrogen concentration. (c) Measurement between mica sheets with the SFA in KNO_3 solutions in the concentration range 0.06–1.0 M [70]. The fitted Hamaker constants are in (a) 1.7×10^{-21} J, in (b) 3.3×10^{-21} J, and in (c) 7.8×10^{-21} J.

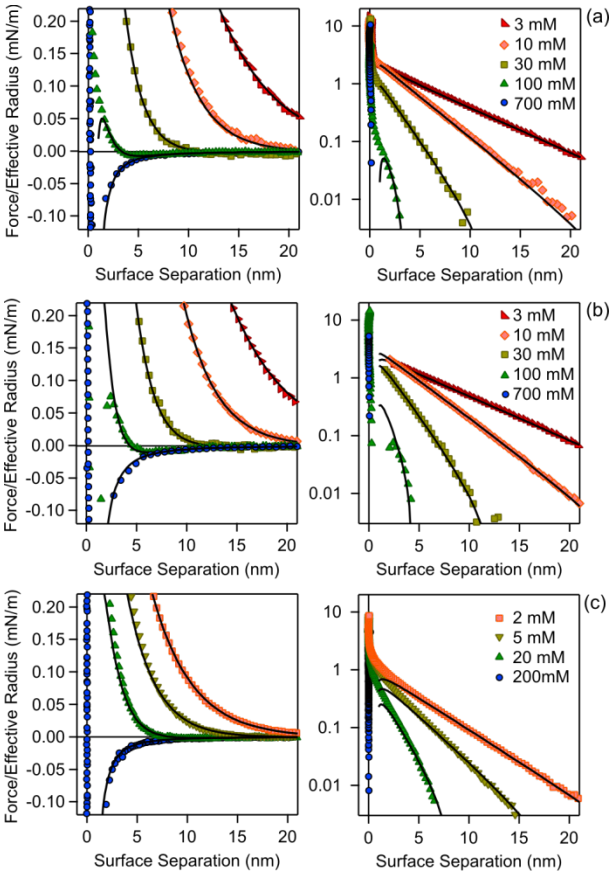

Figure 3. Typical force profiles for various substrates in different electrolytes. Left column shows the linear representation and right column the semi-logarithmic one. Solid lines are best fits with DLVO theory with non-retarded van der Waals force and DH superposition approximation. (a) Silica and (b) sulfate polystyrene latex in KCl solution of pH 4.0 and (c) silica in $MgSO_4$ solution at pH 5.6. Adapted from Refs. [66,68].

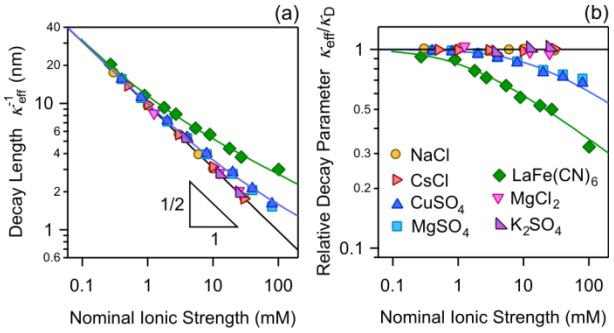

Figure 4. Comparison of measured inverse decay lengths versus the nominal ionic strength. The latter quantity is calculated by assuming full dissociation. The solid lines represent either predictions of DH theory or they illustrate the effect of the ion pairing equilibrium given in eq. (7) with association constants of 2.0×10^2 M^{-1} and 5.0×10^3 M^{-1}. (a) Effective decay length and (b) effective decay parameter relative to the expected Debye parameter.

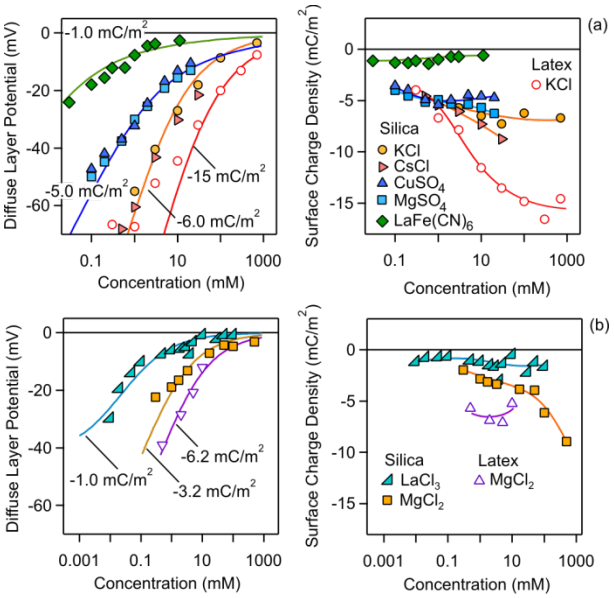

Figure 5. Charging characteristics of various negatively charge substrates [66,78]. Diffuse layer potential is shown in the left column, and the solid lines reflect best fits with a constant charge density as indicated. Corresponding charge density is shown in the right column, whereby the solid lines serve to guide the eye only. (a) Symmetric electrolytes at pH 5.6 and KCl at pH 4.0. (b) Asymmetric electrolytes at pH 4.0.

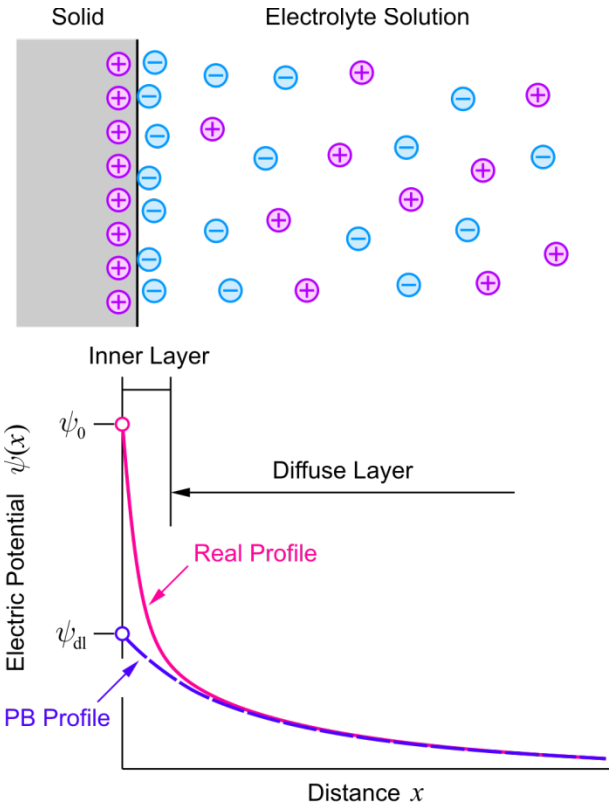

Figure 6. Scheme of the solid-water interface with the inner layer and the diffuse layer together with the corresponding electric potential profile $\psi(x)$ for a positively charged interface. The interface has the bare potential ψ_0. Within the inner layer close to the interface, the potential decays rapidly. At larger distances, the potential decays more slowly. This profile can be well described with the PB model, and is characterized with an appropriate diffuse layer potential ψ_{dl}.

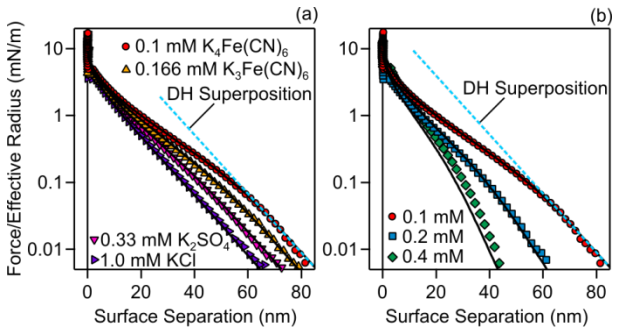

Figure 7. Forces between negatively charged polystyrene latex particles in various 1:z electrolytes at pH 5.6. The multivalent coions have the same sign of charge as the interface. Solid lines are best fits with the PB model. Dashed lines correspond to the DH superposition approximation, eq. (4). The decay length is calculated with eq. (5) by assuming complete dissociation. (a) Electrolytes of an ionic strength of 1.0 mM where the valence of the coion is varied. (b) Variation of the solution concentration of $K_4Fe(CN)_6$. Adapted from Ref. [90].

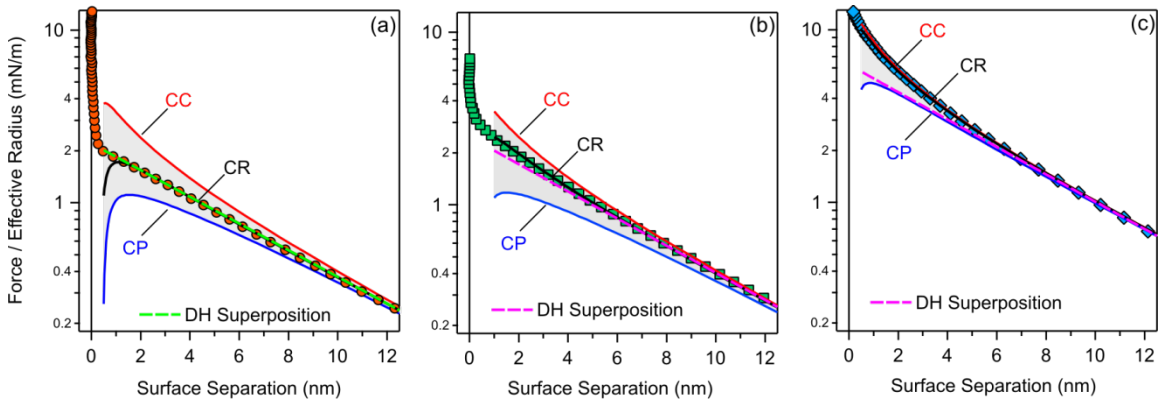

This is a double column figure. Do not print this text.

Figure 8. Force profiles between silica particles in different monovalent salt solutions of a concentration of 3 mM and different pH values. The solid line is the best fit with DLVO theory, which includes the PB model with constant regulation (CR) approximation, from which the regulation parameter p is extracted. The dotted line is the DH superposition approximation. The shaded region is bounded by constant charge (CC, $p = 1$) and constant potential (CP, $p = 0$) cases. (a) CsCl and pH 4.0 with $\psi_{dl} = -41$ mV and $p = 0.45$, (b) LiCl and pH 4.0 with $\psi_{dl} = -43$ mV and $p = 0.69$, and (c) CsCl and pH 10 with $\psi_{dl} = -84$ mV and $p = 0.91$. Adapted from Ref. [142].

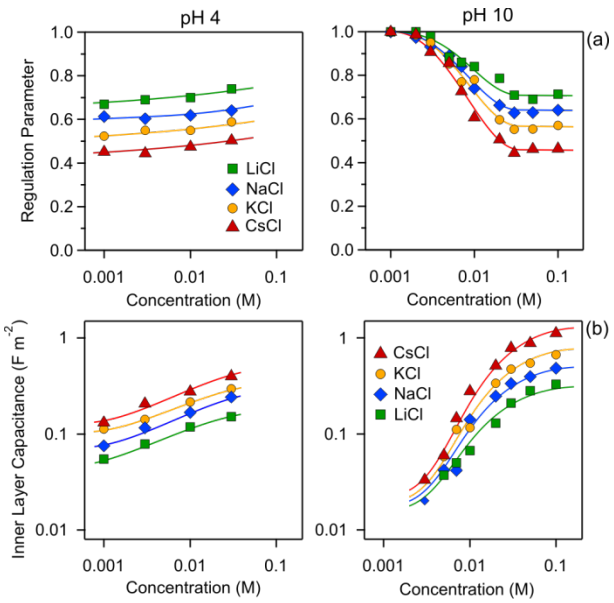

Figure 9. Regulation properties extracted from direct force measurements in monovalent electrolytes. Solid lines serve to guide the eye only. Left column shows data measured at pH 4, and right column at pH 10. (a) Regulation parameter p and (b) inner capacitance C_{in}. Adapted from Ref. [142].

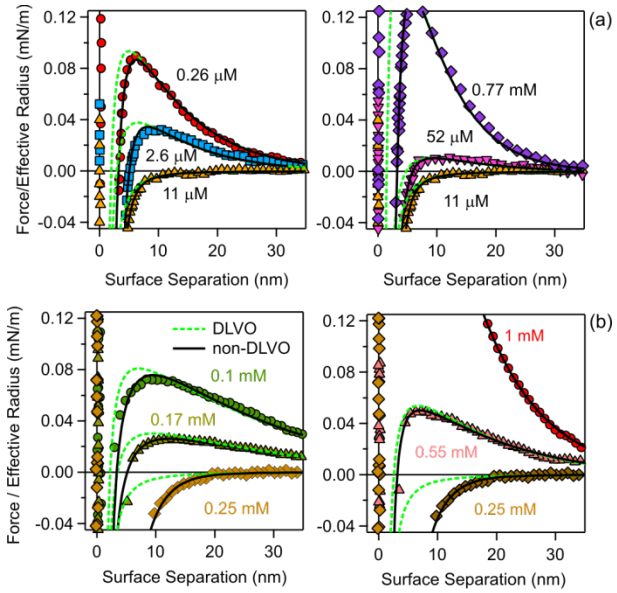

Figure 10. Interaction forces between sulfate latex particles undergoing charge reversal due to the presence of strongly adsorbing counter-ions at pH 4.0. Dashed lines are best fits with DLVO theory involving the PB model with CR, while the solid lines include an additional non-DLVO attraction. (a) Polyamine N6 [69] and (b) Ph_4AsCl [68]. For the explanation of the acronyms see caption of Fig. 2.

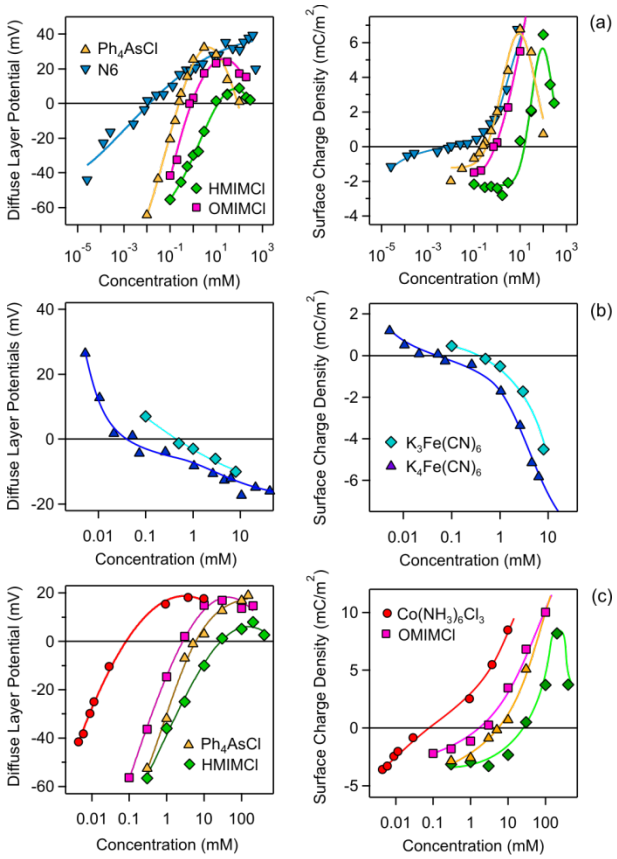

Figure 11. Charging characteristics of various substrates undergoing a charge reversal induced by strongly adsorbing counter-ions. Diffuse layer potential is shown in the left column and the inner layer charge density in the right column. Solid lines serve to guide the eye only. (a) Sulfate latex in the presence of various organic ions [68,69]. (b) Amidine latex in the presence of $K_3Fe(CN)_6$ and $K_4Fe(CN)_6$ [75,77]. (c) Silica particles in the presence of various cations [68,112]. For the explanation of the acronyms see caption of Fig. 2.

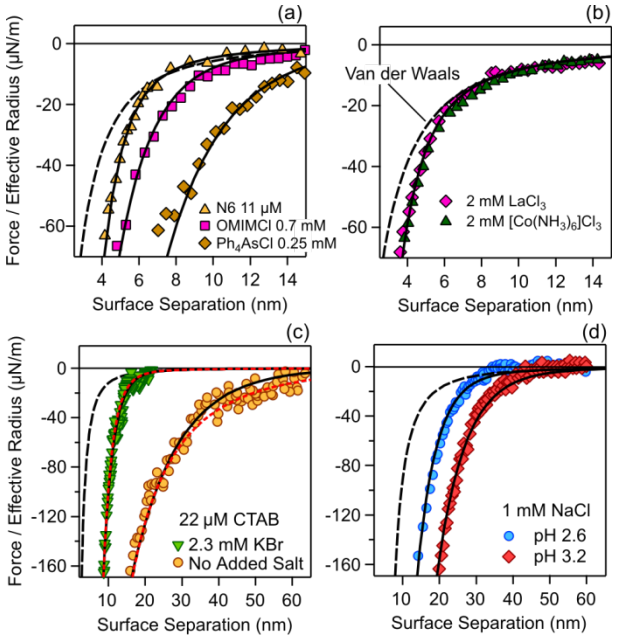

Figure 12. Additional non-DLVO attraction acting between surfaces neutralized by adsorption of oppositely charged ions. Solid lines are best fits when the exponential force given in eq. (14) is added to the van der Waals force. (a) Organic ions with $q^{-1} =$ 1.0 nm for N6, 1.8 nm for OMIM, and 3.0 nm for Ph_4AsCl [68,69], (b) multivalent metal ions with $q^{-1} =$ 1.0 nm [107], (c) cationic surfactant with $q^{-1} =$ 3.1 nm with added salt and 32 nm without [108], and (d) fatty acid with $q^{-1} =$ 6.2 nm at pH 2.6 and 7.4 nm at pH 3.2 [109]. For the explanation of the acronyms see caption of Fig. 2. The dotted lines in (c) show the best fits when eq. (16) used is added to the van der Waals force. The fitted decay lengths are close $\kappa_D^{-1}/2$ in (c) and to κ_D^{-1} in (d), while they are about 5-times smaller than κ_D^{-1} in (a,b).

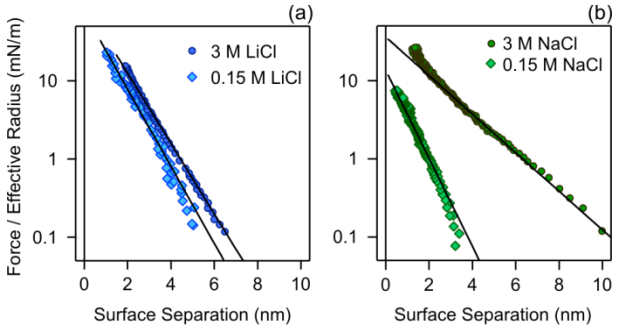

Figure 13. Repulsive non-DLVO forces in concentrated electrolyte solutions near pH 5.6. Solid lines are best fits with the exponential repulsion given by eq. (14). Note that the larger decay length is larger in the more concentrated electrolyte. (a) LiCl [21] and (b) NaCl [22].

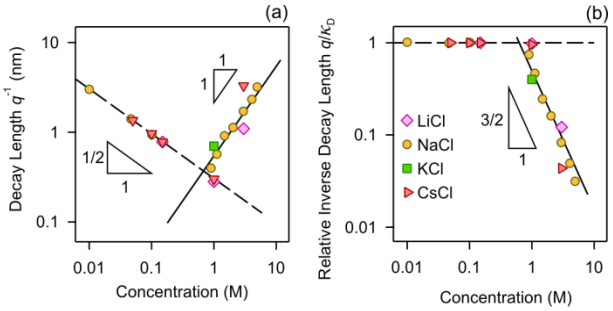

Figure 14. Comparison of measured inverse decay lengths in concentrated monovalent electrolytes. The dashed lines represent either predictions of DH theory and the solid lines of the scaling law given in eq. (17) with $\nu = 3/2$ and ionic diameter $a = 0.4$ nm. The actual diameters are expected to be lower due to dielectric effects. (a) Measured decay length and (b) inverse decay length relative to the expected Debye length.

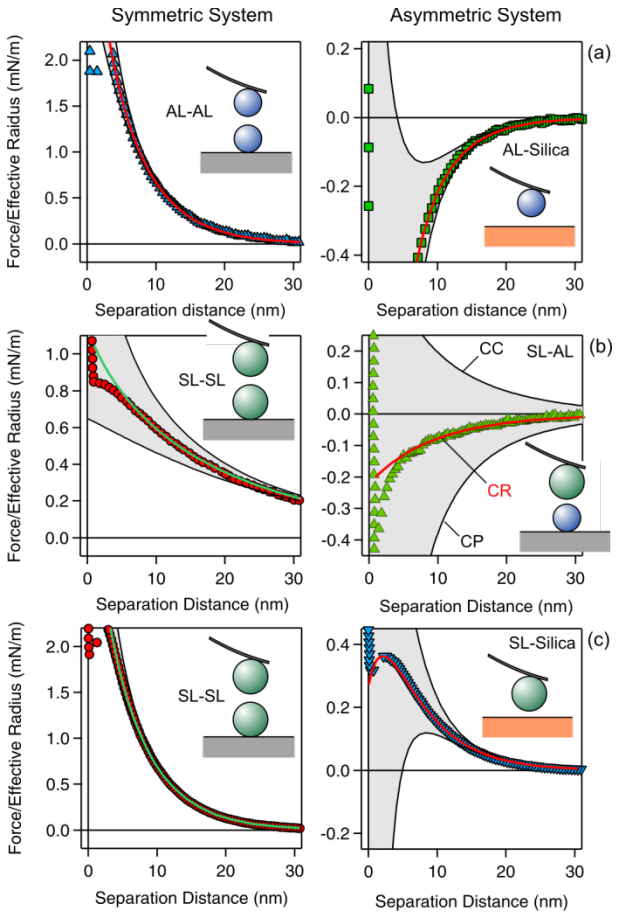

Figure 15. Force measurements in symmetric (left column) and asymmetric systems (right column). One of the surfaces in the asymmetric setting is used to realize the symmetric setting. Solid lines are best fits with the PB model with CR approximation. The grey region is delimited with the respective results that use CC and CP boundary conditions. Interactions involving a planar silica substrate with $\psi_{dl} = -13$ mV and $p = 0.31$ in 2 mM KCl solution at pH 3.0 with (a) oppositely charged amidine latex particles with $\psi_{dl} = +59$ mV and $p = 0.37$ and (c) with like-charged sulfate latex particles with $\psi_{dl} = -60$ mV and $p = 0.31$ [134]. (b) The charge-neutral case was realized with negatively charged sulfate particles with $\psi_{dl} = -54$ mV and $p = 0.48$ and a neutral amidine particle with $p = 0.33$ in 0.2 mM KCl solution at pH 5.6 [135].

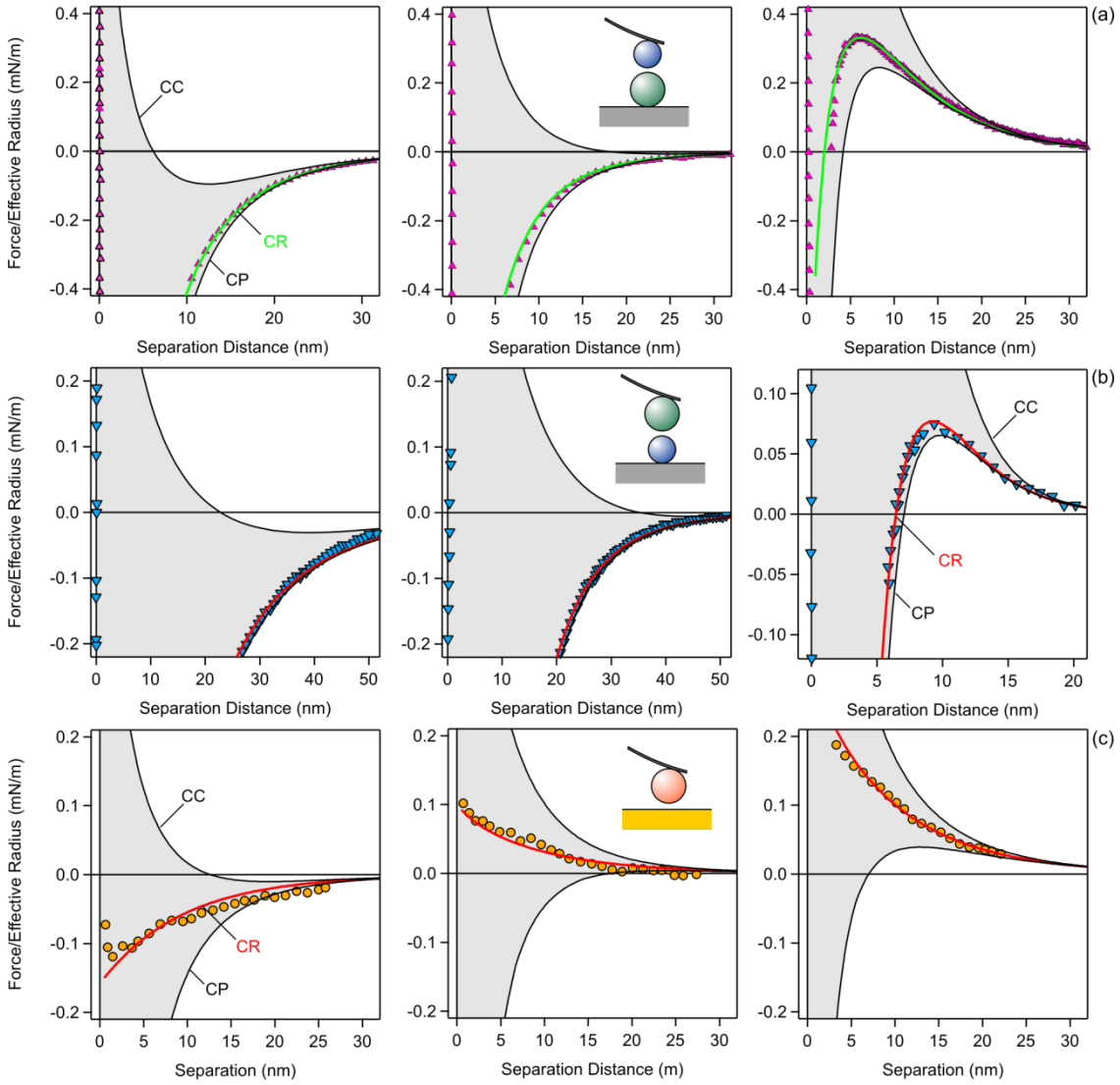

This is a double column figure. Do not print this text.

Figure 16. Charge reversal probed by direct force measurements in the asymmetric setting. Thereby one of the surfaces is highly charged, while the other one undergoes a charge reversal. Forces between the highly charged surfaces were further measured in the symmetric setting to extract the respective surface parameters. Solid lines are best fits with the PB model with CR approximation. The grey region is delimited with the respective results that use CC and CP boundary conditions. (a) Sulfate particles with $\psi_{dl} = -20$, –3.5, and +21 mV (left to right) and $p = 0.13$ and amidine particles with $\psi_{dl} = +61 \pm 6$ mV and $p = 0.38$ in solutions of a polyamine N6 of concentrations 3.0, 11, and 770 µM (left to right) at pH 4.0 [98]. Further details concerning N6 are given in the caption of Fig. 2. (b) Amidine particles with $\psi_{dl} = +15$, –3.7, and –7.2 mV (left to right) and $p = 0.07$ and sulfate particles with $\psi_{dl} = -90 \pm 10$ mV and $p = 0.37$ in solutions of potassium ferrocyanide $K_4Fe(CN)_6$ of concentrations 0.01, 0.05, and 1.0 mM at pH 4.0 [77]. (c) Interactions between a gold surface under potentiostatic control with $\psi_{dl} = +4.7$, –2.9, and –9.2 mV (left to right) and $p = 0.49$ and a silica particle with $\psi_{dl} = -36$ mV and $p = 0.72$ in 1 mM KCl solutions of pH 5.5 [55]. The applied electrode potentials versus the saturated calomel electrode are 0, –100, and –200 mV (left to right). The published force profiles were corrected with a common linear baseline.

References

[1] B. Derjaguin, L. D. Landau, Acta Phys. Chim. 14 (1941) 633-662.

[2] E. J. W. Verwey, J. T. G. Overbeek, Theory of Stability of Lyophobic Colloids, Elsevier, Amsterdam, 1948.

[3] W. B. Russel, D. A. Saville, W. R. Schowalter, Colloidal Dispersions, Cambridge University Press, Cambridge, 1989.

[4] M. Elimelech, J. Gregory, X. Jia, R. A. Williams, Particle Deposition and Aggregation: Measurement, Modeling, and Simulation, Butterworth-Heinemann Ltd., Oxford, 1995.

[5] J. Israelachvili, Intermolecular and Surface Forces, Academic Press, London, 2011.

[6] G. L. Klimchitskaya, U. Mohideen, V. M. Mostepanenko, Rev. Mod. Phys. 81 (2009) 1827-1885.

[7] B. Derjaguin, Acta Phys. Chim. 10 (1939) 333-346.

[8] I. Langmuir, J. Chem. Phys. 6 (1938) 873-896.

[9] B. W. Ninham, V. A. Parsegian, J. Theor. Biol. 31 (1971) 405-408.

[10] L. Guldbrand, B. Jonsson, H. Wennerstrom, P. Linse, J. Chem. Phys. 80 (1984) 2221-2228.

[11] R. Kjellander, S. Marcelja, J. Chem. Phys. 82 (1985) 2122-2135.

[12] A. Naji, M. Kanduc, J. Forsman, R. Podgornik, J. Chem. Phys. 139 (2013) 150901.

[13] M. Z. Bazant, B. D. Storey, A. A. Kornyshev, Phys. Rev. Lett. 106 (2011) 046102.

[14] A. C. Maggs, R. Podgornik, Soft Matter 12 (2016) 1219-1229.

[15] W. A. Ducker, D. Mastropietro, Curr. Opin. Colloid Interface Sci. 22 (2016) 51-58.

[16] R. F. Tabor, F. Grieser, R. R. Dagastine, D. Y. C. Chan, Phys. Chem. Chem. Phys. 16 (2014) 18065-18075.

[17] J. Israelachvili, R. Pashley, Nature 300 (1982) 341-342.

[18] S. J. Miklavic, D. Y. C. Chan, L. R. White, T. W. Healy, J. Phys. Chem. 98 (1994) 9022-9032.

[19] R. M. Adar, D. Andelman, H. Diamant, Adv. Colloid Interface Sci. 247 (2017) 198-207.

[20] M. A. Gebbie, A. M. Smith, H. A. Dobbs, A. A. Lee, G. G. Warr, X. Banquy, M. Valtiner, M. W. Rutland, J. N. Israelachvili, S. Perkin, R. Atkin, Chem. Commun. 53 (2017) 1214-1224.

[21] T. Baimpos, B. R. Shrestha, S. Raman, M. Valtiner, Langmuir 30 (2014) 4322-4332.

[22] A. M. Smith, A. A. Lee, S. Perkin, J. Phys. Chem. Lett. 7 (2016) 2157-2163.

[23] J. T. G. Overbeek, M. J. Sparnaay, J. Colloid Sci. 7 (1952) 343-345.

[24] B. V. Derjaguin, A. S. Titijevskaia, Abricossova, II, A. D. Malkina, Disc. Faraday Soc. (1954) 24-41.

[25] D. Tabor, R. H. S. Winterton, Proc. R. Soc. Lond. A 312 (1969) 435-450.

[26] J. Israelachvili, D. Tabor, Proc. R. Soc. Lond. A 331 (1972) 19-38.

[27] J. Israelachvili, Y. Min, M. Akbulut, A. Alig, G. Carver, W. Greene, K. Kristiansen, E. Meyer, N. Pesika, K. Rosenberg, H. Zeng, Rep. Prog. Phys. 73 (2010) 036601.

[28] H. J. Butt, Biophys. J. 60 (1991) 1438-1444.
[29] W. A. Ducker, T. J. Senden, R. M. Pashley, Nature 353 (1991) 239-241.
[30] D. C. Prieve, N. A. Frej, Langmuir 6 (1990) 396-403.
[31] D. C. Prieve, Adv. Colloid Interface Sci. 82 (1999) 93-125.
[32] G. Volpe, T. Brettschneider, L. Helden, C. Bechinger, Opt. Express 17 (2009) 23975-23985.
[33] J. C. Crocker, D. G. Grier, Phys. Rev. Lett. 73 (1994) 352-355.
[34] C. Gutsche, U. F. Keyser, K. Kegler, F. Kremer, Phys. Rev. E 76 (2007) 031403.
[35] J. Dobnikar, M. Brunner, H. H. von Grunberg, C. Bechinger, Phys. Rev. E 69 (2004) 031402.
[36] X. C. Xing, L. Hua, T. Ngai, Curr. Opin. Colloid Interface Sci. 20 (2015) 54-59.
[37] I. Szilagyi, G. Trefalt, A. Tiraferri, M. Borkovec, Soft Matter 10 (2014) 2479-2502.
[38] R. von Klitzing, E. Thormann, T. Nylander, D. Langevin, C. Stubenrauch, Adv. Colloid Interface Sci. 155 (2010) 19-31.
[39] M. F. Hsu, E. R. Dufresne, D. A. Weitz, Langmuir 21 (2005) 4881-4887.
[40] F. Waggett, M. D. Shafiq, P. Bartlett, Colloid Interfaces 2 (2018).
[41] B. Derjaguin, Kolloid Z. 69 (1934) 155-164.
[42] L. R. White, J. Colloid Interface Sci. 95 (1983) 286-288.
[43] H. Kawai, H. Sakuma, M. Mizukami, T. Abe, Y. Fukao, H. Tajima, K. Kurihara, Rev. Sci. Instrum. 79 (2008).
[44] T. Kamijo, M. Kasuya, M. Mizukami, K. Kurihara, Chem. Lett. 40 (2011) 674-675.
[45] J. Frechette, T. K. Vanderlick, Langmuir 17 (2001) 7620-7627.
[46] M. Kasuya, T. Sogawa, T. Masuda, T. Kamijo, K. Uosaki, K. Kurihara, J. Phys. Chem. C 120 (2016) 15986-15992.
[47] M. Valtiner, X. Banquy, K. Kristiansen, G. W. Greene, J. N. Israelachvili, Langmuir 28 (2012) 13080-13093.
[48] R. Tivony, J. Klein, Langmuir 32 (2016) 7346-7355.
[49] E. Kumacheva, J. Klein, J. Chem. Phys. 108 (1998) 7010-7022.
[50] M. Heuberger, Rev. Sci. Instrum. 72 (2001) 1700-1707.
[51] G. Toikka, R. A. Hayes, J. Ralston, Langmuir 12 (1996) 3783-3788.
[52] I. Larson, C. J. Drummond, D. Y. C. Chan, F. Grieser, J. Phys. Chem. 99 (1995) 2114-2118.
[53] D. Ebeling, D. van den Ende, F. Mugele, Nanotechnology 22 (2011) 305706.
[54] N. Helfricht, A. Mark, L. Dorwling-Carter, T. Zambelli, G. Papastavrou, Nanoscale 9 (2017) 9491-9501.
[55] A. C. Hillier, S. Kim, A. J. Bard, J. Phys. Chem. 100 (1996) 18808-18817.
[56] S. Rentsch, H. Siegenthaler, G. Papastavrou, Langmuir 23 (2007) 9083-9091.
[57] D. Barten, J. M. Kleijn, J. Duval, H. P. van Leeuwen, J. Lyklema, M. A. Cohen Stuart, Langmuir 19 (2003) 1133-1139.

[58] S. R. van Lin, K. K. Grotz, I. Siretanu, N. Schwierz, F. Mugele, Langmuir 35 (2019) 5737-5745.
[59] J. I. Kilpatrick, S. H. Loh, S. P. Jarvis, J. Am. Chem. Soc. 135 (2013) 2628-2634.
[60] T. Fukuma, Y. Ueda, S. Yoshioka, H. Asakawa, Phys. Rev. Lett. 104 (2010) 016101.
[61] M. Nayeri, Z. Abbas, J. Bergenholtz, Colloid Surf. A 429 (2013) 74-81.
[62] J. Baumgartl, C. Bechinger, Europhys. Lett. 71 (2005) 487-493.
[63] M. Ricci, P. Spijker, K. Voitchovsky, Nature Comm. 5 (2014) 4400.
[64] V. Valmacco, M. Elzbieciak-Wodka, C. Besnard, P. Maroni, G. Trefalt, M. Borkovec, Nanoscale Horizons 1 (2016) 325 - 330.
[65] M. Elzbieciak-Wodka, M. Popescu, F. J. Montes Ruiz-Cabello, G. Trefalt, P. Maroni, M. Borkovec, J. Chem. Phys. 140 (2014) 104906.
[66] A. M. Smith, P. Maroni, G. Trefalt, M. Borkovec, J. Phys. Chem. B. 123 (2019) 1733-1740.
[67] M. Dishon, O. Zohar, U. Sivan, Langmuir 25 (2009) 2831-2836.
[68] A. M. Smith, P. Maroni, M. Borkovec, Phys. Chem. Chem. Phys. 20 (2018) 158-164.
[69] M. Moazzami-Gudarzi, G. Trefalt, I. Szilagyi, P. Maroni, M. Borkovec, J. Phys. Chem. C 119 (2015) 15482-15490.
[70] R. M. Espinosa-Marzal, T. Drobek, T. Balmer, M. P. Heuberger, Phys. Chem. Chem. Phys. 14 (2012) 6085-6093.
[71] J. N. Israelachvili, G. E. Adams, J. Chem. Soc. Farad. Trans. I 74 (1978) 975-1001.
[72] H. D. Ackler, R. H. French, Y. M. Chiang, J. Colloid Interface Sci. 179 (1996) 460-469.
[73] N. Eom, D. F. Parsons, V. S. J. Craig, J. Phys. Chem. B 121 (2017) 6442-6453.
[74] Y. Marcus, G. Hefter, Chem. Rev. 106 (2006) 4585-4621.
[75] F. J. Montes Ruiz-Cabello, G. Trefalt, P. Maroni, M. Borkovec, Langmuir 30 (2014) 4551-4555.
[76] A. Tulpar, V. Subramanian, W. Ducker, Langmuir 17 (2001) 8451-8454.
[77] M. Moazzami-Gudarzi, P. Adam, A. M. Smith, G. Trefalt, I. Szilagyi, P. Maroni, M. Borkovec, Phys. Chem. Chem. Phys. 20 (2018) 9436-9448
[78] V. Valmacco, M. Elzbieciak-Wodka, D. Herman, G. Trefalt, P. Maroni, M. Borkovec, J. Colloid Interf. Sci. 472 (2016) 108-115.
[79] P. G. Hartley, I. Larson, P. J. Scales, Langmuir 13 (1997) 2207-2214.
[80] G. Trefalt, I. Szilagyi, M. Borkovec, J. Colloid Interf. Sci. 406 (2013) 111-120.
[81] M. A. Brown, Z. Abbas, A. Kleibert, R. G. Green, A. Goel, S. May, T. M. Squires, Phys. Rev. X 6 (2016) 011007.
[82] M. Kobayashi, M. Skarba, P. Galletto, D. Cakara, M. Borkovec, J. Colloid Interface Sci. 292 (2005) 139-147.
[83] M. A. Brown, A. Goel, Z. Abbas, Angew. Chem. Int. Ed. 55 (2016) 3790-3794.
[84] T. Hiemstra, J. C. M. de Wit, W. H. van Riemsdijk, J. Colloid Interface Sci. 133 (1989) 105-117.
[85] T. Hiemstra, W. H. Van Riemsdijk, J. Colloid Interface Sci. 210 (1999) 182-193.

[86] M. K. Ridley, M. L. Machesky, D. J. Wesolowski, D. A. Palmer, Geochim. Cosmochim. Acta 68 (2004) 239-251.
[87] D. A. Sverjensky, Geochim. Cosmochim. Acta 65 (2001) 3643-3655.
[88] M. M. Hatlo, L. Lue, Soft Matter 5 (2009) 125-133.
[89] A. P. dos Santos, A. Diehl, Y. Levin, J. Chem. Phys. 132 (2010) 104105.
[90] F. J. Montes Ruiz-Cabello, M. Moazzami-Gudarzi, M. Elzbieciak-Wodka, P. Maroni, C. Labbez, M. Borkovec, G. Trefalt, Soft Matter 11 (2015) 1562-1571.
[91] S. L. Carnie, D. Y. C. Chan, J. Colloid Interface Sci. 161 (1993) 260-264.
[92] S. H. Behrens, M. Borkovec, J. Phys. Chem. B 103 (1999) 2918-2928.
[93] G. Trefalt, S. H. Behrens, M. Borkovec, Langmuir 32 (2016) 380-400.
[94] B. V. Zhmud, A. Meurk, L. Bergstrom, J. Colloid Interface Sci. 207 (1998) 332-343.
[95] C. Zhao, D. Ebeling, I. Siretanu, D. van den Ende, F. Mugele, Nanoscale 7 (2015) 16298-16311.
[96] S. H. Behrens, M. Borkovec, J. Chem. Phys. 111 (1999) 382-385.
[97] D. J. Bonthuis, S. Gekle, R. R. Netz, Langmuir 28 (2012) 7679-7694.
[98] M. Moazzami-Gudarzi, G. Trefalt, I. Szilagyi, P. Maroni, M. Borkovec, Phys. Chem. Chem. Phys. 18 (2016) 8739-8751.
[99] P. Kekicheff, S. Marcelja, T. J. Senden, V. E. Shubin, J. Chem. Phys. 99 (1993) 6098-6113.
[100] E. E. Meyer, K. J. Rosenberg, J. Israelachvili, Proc. Natl. Acad. Sci. U. S. A. 103 (2006) 15739-15746.
[101] H. K. Christenson, P. M. Claesson, Adv. Colloid Interface Sci. 91 (2001) 391-436.
[102] S. H. Donaldson, A. Royne, K. Kristiansen, M. V. Rapp, S. Das, M. A. Gebbie, D. W. Lee, P. Stock, M. Valtiner, J. Israelachvili, Langmuir 31 (2015) 2051-2064.
[103] D. J. Mastropietro, W. A. Ducker, Phys. Rev. Lett. 108 (2012) 106101.
[104] S. Naserifar, W. A. Goddard, Proc. Natl. Acad. Sci. U. S. A. 116 (2019) 1998-2003.
[105] A. Carambassis, L. C. Jonker, P. Attard, M. W. Rutland, Phys. Rev. Lett. 80 (1998) 5357-5360.
[106] V. S. J. Craig, Soft Matter 7 (2011) 40-48.
[107] M. Dishon, O. Zohar, U. Sivan, Langmuir 27 (2011) 12977-12984.
[108] P. Kekicheff, O. Spalla, Phys. Rev. Lett. 75 (1995) 1851-1854.
[109] N. Eom, D. F. Parsons, V. S. J. Craig, Soft Matter 13 (2017) 8910-8921.
[110] F. J. Montes Ruiz-Cabello, G. Trefalt, Z. Csendes, P. Sinha, T. Oncsik, I. Szilagyi, P. Maroni, M. Borkovec, J. Phys. Chem. B 117 (2013) 11853-11862.
[111] P. Sinha, I. Szilagyi, F. J. Montes Ruiz-Cabello, P. Maroni, M. Borkovec, J. Phys. Chem. Lett. 4 (2013) 648-652.
[112] O. Zohar, I. Leizerson, U. Sivan, Phys. Rev. Lett. 96 (2006) 177802.
[113] J. Zhang, R. H. Yoon, M. Mao, W. A. Ducker, Langmuir 21 (2005) 5831-5841.
[114] D. Ben-Yaakov, D. Andelman, H. Diamant, Phys. Rev. E 87 (2013) 022402.

[115] G. Silbert, D. Ben-Yaakov, Y. Dror, S. Perkin, N. Kampf, J. Klein, Phys. Rev. Lett. 109 (2012) 168305.
[116] P. Kekicheff, J. Iss, P. Fontaine, A. Johner, Phys. Rev. Lett. 120 (2018) 118001.
[117] J. G. Kirkwood, J. B. Shumaker, Proc. Natl. Acad. Sci. U. S. A. 38 (1952) 863-871.
[118] O. Spalla, L. Belloni, Phys. Rev. Lett. 74 (1995) 2515-2518.
[119] R. Podgornik, J. Chem. Phys. 91 (1989) 5840-5849.
[120] P. Kekicheff, Adv. Colloid Interf. Sci. 270 (2019) 191-215.
[121] N. Adzic, R. Podgornik, Phys. Rev. E 91 (2015) 022715.
[122] N. Ishida, K. Matsuo, K. Imamura, V. S. J. Craig, Langmuir 34 (2018) 3588-3596.
[123] P. Stock, T. Utzig, M. Valtiner, J. Colloid Interface Sci. 446 (2015) 244-251.
[124] M. Kanduc, A. Schlaich, E. Schneck, R. R. Netz, Langmuir 32 (2016) 8767-8782.
[125] Q. Y. Hu, C. Weber, H. W. Cheng, F. U. Renner, M. Valtiner, ChemPhysChem 18 (2017) 3056-3065.
[126] G. Vigil, Z. H. Xu, S. Steinberg, J. Israelachvili, J. Colloid Interface Sci. 165 (1994) 367-385.
[127] B. C. Donose, I. U. Vakarelski, K. Higashitani, Langmuir 21 (2005) 1834-1839.
[128] S. M. Acuna, P. G. Toledo, J. Colloid Interface Sci. 361 (2011) 397-399.
[129] Y. H. Wang, L. G. Wang, M. A. Hampton, A. V. Nguyen, J. Phys. Chem. C 117 (2013) 2113-2120.
[130] M. A. Gebbie, H. A. Dobbs, M. Valtiner, J. N. Israelachvili, Proc. Natl. Acad. Sci. U. S. A. 112 (2015) 7432-7437.
[131] A. A. Lee, C. S. Perez-Martinez, A. M. Smith, S. Perkin, Phys. Rev. Lett. 119 (2017) 026002.
[132] R. M. Adar, S. A. Safran, H. Diamant, D. Andelman, J. Chem. Phys. (2019) (in press).
[133] B. Rotenberg, O. Bernard, J. P. Hansen, J. Phys. Condes. Matter 30 (2018) 054005.
[134] F. J. Montes Ruiz-Cabello, G. Trefalt, P. Maroni, M. Borkovec, Phys. Rev. E 90 (2014) 012301.
[135] I. Popa, P. Sinha, M. Finessi, P. Maroni, G. Papastavrou, M. Borkovec, Phys. Rev. Lett. 104 (2010) 228301.
[136] K. Besteman, M. A. G. Zevenbergen, H. A. Heering, S. G. Lemay, Phys. Rev. Lett. 93 (2004) 170802.
[137] R. Tivony, D. Ben Yaakov, G. Silbert, J. Klein, Langmuir 31 (2015) 12845-12849.
[138] M. A. Gebbie, M. Valtiner, X. Banquy, E. T. Fox, W. A. Henderson, J. N. Israelachvili, Proc. Natl. Acad. Sci. U. S. A. 110 (2013) 9674-9679.
[139] J. P. Fitts, T. P. Trainor, D. Grolimund, J. R. Bargar, G. A. Parks, G. E. Brown, J. Synchrot. Radiat. 6 (1999) 627-629.
[140] M. Porus, C. Labbez, P. Maroni, M. Borkovec, J. Chem. Phys. 135 (2011) 064701.
[141] S. Rode, N. Oyabu, K. Kobayashi, H. Yamada, A. Kuhnle, Langmuir 25 (2009) 2850-2853.
[142] A. M. Smith, P. Maroni, M. Borkovec, G. Trefalt, Colloids Interfaces 2 (2018) 65.